Adiabatic theory of generation and rescattering of vortex electrons in strong-field ionization by elliptically polarized pulses

Kirill V. Bazarov [1,2,*] and Oleg I. Tolstikhin [1,†]

[1]*Moscow Institute of Physics and Technology, Dolgoprudny 141700, Russia*
[2]*NRC "Kurchatov Institute", Moscow 123182, Russia*

The adiabatic theory of strong-field ionization is extended to the specific configuration in which ionization occurs from a vortex orbital in an axially symmetric target by an elliptically polarized pulse with small ellipticity and the major axis of the polarization ellipse directed along the vortex axis of the initial state. Generation of vortex electrons in the continuum, their propagation in the laser field, and subsequent rescattering on the parent ion are described. Adiabatic asymptotics of the rescattering parts of the solution to the time-dependent Schrödinger equation and the ionization amplitude are obtained. On the basis of these results, the factorization formula giving the photoelectron momentum distribution (PEMD) in the vicinity of a backward rescattering caustic is derived. Our interest in the present configuration stems from the fact that, because of the nonzero ellipticity of the field, liberated vortex electrons arrive for rescattering with a nonzero impact parameter. The corresponding scattering amplitude generalizes the recently introduced vortex scattering amplitude characterizing head-on vortex-target rescattering in the linear polarization case [O. I. Tolstikhin and T. Morishita, Phys. Rev. A **99**, 063415 (2019)]. Using the factorization formula, one can extract the absolute value of this generalized scattering amplitude from the observable PEMD, which opens a new window for target structure imaging in strong-field physics. The theory is illustrated by calculations for two atomic targets, $He^+(2p, m = 1)$ and $Xe(5p, m = 1)$. We show that in the case of the initial π orbital and nonzero ellipticity not only the absolute values of two head-on scattering amplitudes with $m = 0$ and 1, but also their phase difference as functions of the scattering angle can be extracted from the PEMD.

I. INTRODUCTION

An electron liberated from an atom or a molecule by a strong laser field returns to the parent ion and undergoes rescattering [1]. The rescattered electron carries information about the target structure, and this information is thus encoded in the observable photoelectron momentum distribution (PEMD) [2]. Rescattering photoelectron spectroscopy aims at extracting this information from the PEMD. In particular, a fruitful approach enabling one to extract the differential cross section (DCS) for elastic electron-parent ion collision was proposed [3] and demonstrated [4–16]. This approach is based on the observation that in the region of the photoelectron momentum space dominated by rescattered photoelectrons the PEMD factorizes into the DCS and a returning photoelectron wave packet (RWP) [3,17–20]. The factorization formula for the PEMD was derived and the explicit analytical expression for the RWP was obtained within the adiabatic theory of strong-field ionization [21] in Ref. [22], which has elevated the approach initiated in Ref. [3] to a quantitative level [23–27].

Recently, the theory of Ref. [22] has been extended to target structure imaging with vortex electrons [28]. In a vortex state an electron has a nonzero projection of its orbital

angular momentum on a given axis. Bound states in axially symmetric potentials characterized by a nonzero magnetic quantum number give an example of vortex states familiar from atomic and molecular physics. Less familiar vortex states of free electrons have attracted much attention in recent years, reviews on the theory and applications of such states can be found in Refs. [29–31]. Of particular interest in the context of rescattering are papers developing the theory of collisions of vortex electrons with atoms [32–36] and molecules [37]; see also a review article [38] and references therein. The interaction of free vortex electrons with strong electromagnetic fields was considered in Refs. [39,40]. Vortex electrons in strong-field physics, which involves their interaction with both the parent ion and a laser field, were discussed theoretically [28, 41–51]. In experimental studies so far they were detected only indirectly by observing effects due to vorticity of the initial bound [52,53] and final continuum [54–56] states.

Returning to Ref. [28], the imaging procedure using vortex electrons proposed therein is similar to that based on rescattering of plane-wave electrons [22]. The factorization formulas derived in Refs. [22,28] hold in the vicinity of a backward rescattering caustic. Given the PEMD at the caustic and knowing the RWP, one can extract the target-dependent factor describing rescattering. In the plane-wave case, this factor is the DCS given by the absolute value squared of the usual scattering amplitude known from scattering theory [57,58]. In the case of vortex rescattering, this factor is the

---

*bazarov.kv@phystech.edu
†tolstikhin.oi@mipt.ru

053114-1

absolute value squared of a generalized scattering amplitude. In the configuration analyzed in Ref. [28], vortex electrons are generated in strong-field ionization from an initial vortex orbital by a laser field linearly polarized along its axis. In this case the vortex axis is conserved in time and photoelectrons undergo head-on vortex rescattering on the parent ion. The scattering amplitude characterizing this process in the adiabatic regime was introduced in Ref. [28]. The absolute value of this amplitude can be extracted from the PEMD. Note that while the DCS in principle can be measured independently in collision experiments, the head-on vortex scattering amplitude is accessible only through the imaging procedure discussed in Ref. [28].

In this paper we further extend the theory of Refs. [22,28] to the configuration in which strong-field ionization occurs from a vortex orbital by an elliptically polarized laser pulse. In contrast to the linear polarization case [28], in the case of elliptic polarization liberated vortex electrons return for rescattering with a nonzero impact parameter. The corresponding scattering amplitude generalizes the head-on vortex scattering amplitude introduced in Ref. [28]. This amplitude is encoded in the PEMD. Our goal is to show that the target structure information represented by this amplitude can be extracted from the PEMD.

The paper is organized as follows. In Sec. II, we discuss the specificity of the present configuration in the general context of the adiabatic theory [21]. To describe strong-field ionization from a vortex orbital by an eclipticaly polarized field the theory should be redeveloped. Tunneling ionization, propagation, and rescattering stages of strong-field ionization dynamics should be reconsidered. This is done in Secs. III–V, respectively. Based on the results obtained, in Sec. VI we derive the factorization formula for the present configuration. In Sec. VII, we illustrate the theory by calculations for two atomic targets, $He^+(2p, m = 1)$ and $Xe(5p, m = 1)$. Section VIII concludes the paper. A method to calculate vortex scattering amplitudes for spherically symmetric potentials is presented in the Appendix.

II. FORMULATION OF THE PROBLEM

Consider an electron interacting with a target potential $V(\mathbf{r})$ and a strong laser field $\mathbf{F}(t)$. The time-dependent Schrödinger equation describing the system in the dipole approximation and length gauge reads (atomic units are used throughout)

$$i\frac{\partial \psi(\mathbf{r},t)}{\partial t} = \left[-\frac{1}{2}\Delta + V(\mathbf{r}) + \mathbf{F}(t)\mathbf{r}\right]\psi(\mathbf{r},t). \quad (1)$$

The field is assumed to satisfy $\mathbf{F}(t \to \pm\infty) = \mathbf{0}$. The initial condition for Eq. (1) is

$$\psi(\mathbf{r}, t \to -\infty) = \phi_0(\mathbf{r})e^{-iE_0 t}, \quad (2)$$

where $E_0 < 0$ and $\phi_0(\mathbf{r})$ are the energy and wave function of a bound state of the field-free target. The interaction with the field causes ionization of the target. The amplitude of ionization with photoelectron momentum $\mathbf{k}$ is given by

$$I(\mathbf{k}) = \int \left[\psi_{\mathbf{k}}^{(-)}(\mathbf{r})e^{-i\mathbf{k}^2 t/2}\right]^* \psi(\mathbf{r},t)d\mathbf{r}|_{t\to\infty}, \quad (3)$$

where $\psi_{\mathbf{k}}^{(-)}(\mathbf{r})$ is the *out* scattering state of the field-free target with asymptotic momentum $\mathbf{k}$ normalized by $\langle\psi_{\mathbf{k}}^{(-)}|\psi_{\mathbf{k}'}^{(-)}\rangle = (2\pi)^3\delta(\mathbf{k} - \mathbf{k}')$ [57,58]. It defines the observable PEMD

$$P(\mathbf{k}) = |I(\mathbf{k})|^2. \quad (4)$$

The evaluation and analysis of this function for different target potentials and fields is one of the central problems in strong-field physics [59].

The adiabatic theory developed in Ref. [21] amounts to the asymptotic solution of this problem in the limit

$$\epsilon \to 0, \quad (5)$$

where ϵ is the adiabatic parameter given by the ratio of time scales characterizing electronic motion in the target and variation of the field. For neutral targets in the ground state ($|E_0| \sim 0.5$) and low-frequency laser pulses typically used in strong-field physics ($\omega \sim 0.057$) this parameter can be estimated as $\epsilon \sim \omega/|E_0| \sim 0.1$, which belongs to the adiabatic regime. In the adiabatic approximation the solution to Eq. (1) can be presented in the form [21]

$$\psi(\mathbf{r}, t) = \psi_a(\mathbf{r}, t) + \psi_r(\mathbf{r}, t). \quad (6)$$

The adiabatic part $\psi_a(\mathbf{r}, t)$ of the wave function describes the initial bound state distorted by the instantaneous laser field $\mathbf{F}(t)$ and adiabatically following its variation in time. Electrons liberated from the target by tunneling through a barrier formed by the target potential and the field are described by the outgoing wave in the asymptotic part of $\psi_a(\mathbf{r}, t)$. The rescattering part $\psi_r(\mathbf{r}, t)$ of the wave function describes liberated electrons which after propagation driven by the field return to the target for rescattering. The division of $\psi(\mathbf{r}, t)$ into the adiabatic and rescattering parts is justified in the limit (5) by the fact that the two terms in Eq. (6) have amplitudes $O(\epsilon^0)$ and $O(\epsilon^{3/2})$ and phases $O(\epsilon^{-1})$ and $O(\epsilon^{-3})$, respectively. Equation (6) holds in the quasistationary zone whose radius scales as $O(\epsilon^{-2})$. Substituting Eq. (6) into Eq. (3) gives

$$I(\mathbf{k}) = I_a(\mathbf{k}) + I_r(\mathbf{k}). \quad (7)$$

The adiabatic part $I_a(\mathbf{k})$ of the ionization amplitude describes direct electrons which do not interact with the target after tunneling. The rescattering part $I_r(\mathbf{k})$ of the ionization amplitude describes electrons which undergo rescattering before arriving at the detector measuring the PEMD. Explicit formulas giving the asymptotics of all the terms in Eqs. (6) and (7) in the adiabatic regime (5) were obtained in Ref. [21].

The adiabatic theory applies to arbitrary potential, initial state, and polarization of the laser field. However, while the asymptotics of the adiabatic parts $\psi_a(\mathbf{r}, t)$ and $I_a(\mathbf{k})$ obtained in Ref. [21] are generally valid, the asymptotics of the rescattering parts $\psi_r(\mathbf{r}, t)$ and $I_r(\mathbf{k})$ involve an additional assumption which does not hold in certain specific situations. Namely, the derivation in Ref. [21] assumes that an electron arriving for rescattering is represented by a plane wave. But this is not the case, e.g., for rescattering of vortex electrons generated in the configuration analyzed in Ref. [28].

In this paper we consider a more general configuration. We assume that the potential in Eq. (1) is axially symmetric about the z axis of the laboratory coordinate frame and the initial bound state in Eq. (2) has a nonzero projection $M > 0$ of the

angular momentum on this axis,

$$V(\mathbf{r}) = V(r_\perp, z), \quad \phi_0(\mathbf{r}) = \phi_0(r_\perp, z)e^{iM\varphi}, \tag{8}$$

where $r_\perp = \sqrt{x^2 + y^2}$. In other words, we consider an atom or a linear molecule aligned along the z axis treated in the single-active-electron approximation. These two specifications are consistent with Ref. [28]. The difference is in the polarization of the laser field. In Ref. [28], the field was assumed to be linearly polarized along the z axis. In this case, the projection M is conserved in time and the problem admits a simplified treatment. Here, we consider an elliptically polarized pulse,

$$\mathbf{F}(t) = F_0 f(t)(\varepsilon \sin \omega t, 0, \cos \omega t), \tag{9}$$

characterized by the amplitude F_0, frequency ω, ellipticity ε, and envelope $f(t) > 0$ satisfying $\max[f(t)] = 1$. We assume that the ellipticity is small, $\varepsilon \ll 1$. The relation between the ellipticity and adiabatic parameters is specified by

$$\varepsilon = O(\epsilon^2). \tag{10}$$

As shown below, pulses with such a small ellipticity are most interesting from the experimental point of view since this is the case where valuable information on rescattering of vortex electrons is imprinted in the PEMD. The nonzero ellipticity adds flexibility and significantly enriches the scheme of target structure imaging with vortex electrons discussed in Ref. [28]. To extend the analysis of Ref. [28] to elliptically polarized pulses we need to return to the general theory [21] and rederive the asymptotics of $\psi_r(\mathbf{r}, t)$ and $I_r(\mathbf{k})$ for the case of vortex electrons. This problem is treated in Secs. III–V.

III. IONIZATION

In the adiabatic regime, ionization in a slowly varying laser field $\mathbf{F}(t)$ proceeds as if the field were static and equal to its instantaneous value. The adiabatic part in Eq. (6) describing tunneling ionization dynamics is given by [21]

$$\psi_a(\mathbf{r}, t) = \phi(\mathbf{r}; t)e^{-is(t)}, \tag{11}$$

where

$$s(t) = E_0 t + \int_{-\infty}^{t} [E(t') - E_0] \, dt'. \tag{12}$$

Here $E(t) = E(\mathbf{F}(t))$ and $\phi(\mathbf{r}; t) = \phi(\mathbf{r}; \mathbf{F}(t))$ are expressed in terms of the eigenvalue $E(\mathbf{F})$ and eigenfunction $\phi(\mathbf{r}; \mathbf{F})$ of a Siegert state (SS) in a static electric field $\mathbf{F}$ satisfying the stationary Schrödinger equation

$$\left[-\frac{1}{2}\Delta + V(\mathbf{r}) + \mathbf{Fr} - E(\mathbf{F})\right]\phi(\mathbf{r}; \mathbf{F}) = 0 \tag{13}$$

supplemented by the regularity and outgoing-wave boundary conditions [60]. The SS defining $\psi_a(\mathbf{r}, t)$ is the solution to Eq. (13) which coincides with the initial bound state as the field is turned off,

$$E(\mathbf{F})|_{F\to 0} = E_0, \quad \phi(\mathbf{r}; \mathbf{F})|_{F\to 0} = \phi_0(\mathbf{r}). \tag{14}$$

According to Eq. (9), we are interested in fields of the form

$$\mathbf{F} = F(\sin \beta, 0, \cos \beta), \tag{15}$$

where $\beta = O(\varepsilon)$ is a small angle. In this section we analyze the dependence of the structure of the ionization flux described by the outgoing wave in the asymptotic part of

$\phi(\mathbf{r}; \mathbf{F})$ in the direction opposite to that of $\mathbf{F}$ on β, which is needed for the following. We do this assuming that the field $\mathbf{F}$ is sufficiently weak, so that the weak-field asymptotic theory (WFAT) of tunneling ionization [61] applies.

Let us introduce a coordinate frame $(x', y' = y, z')$ rotated with respect to the laboratory frame (x, y, z) by the angle β clockwise in the (x, z) plane, so that the z' axis is directed along $\mathbf{F}$. The ionization flux is described by the asymptotics of the solution to Eq. (13) given by [60,61]

$$\phi(\mathbf{r}; \mathbf{F})|_{z'\to-\infty} = \int A(\mathbf{k}_\perp; \beta)e^{i\mathbf{k}_\perp \mathbf{r}'_\perp} g(z', k_\perp) \frac{d\mathbf{k}_\perp}{(2\pi)^2}, \tag{16}$$

where $\mathbf{r}'_\perp = (x', y')$ and z' are functions of $\mathbf{r}$ defined by the rotation, the function

$$g(z', k_\perp) = \frac{1}{|2Fz'|^{1/4}} \exp\left[\frac{iF^{1/2}|2z'|^{3/2}}{3} - \frac{i(\varkappa^2 + k_\perp^2)|z'|^{1/2}}{(2F)^{1/2}}\right] \tag{17}$$

represents a wave going away from the target in the direction of $-\mathbf{F}$, and $A(\mathbf{k}_\perp; \beta)$ is the transverse momentum distribution (TMD) amplitude defining the structure of the ionization flux in the plane (x', y') perpendicular to $\mathbf{F}$. The appearance of $\varkappa = \sqrt{2|E_0|}$ in Eq. (17) in the weak-field case results from the first of Eqs. (14). Within the WFAT, the TMD amplitude is given by [61]

$$A(\mathbf{k}_\perp; \beta) = \frac{2i\pi^{1/2}}{F^{1/2}} \sum_\nu f_\nu(\beta)\phi_\nu^{(0)}\left(\frac{k_\perp^2}{F}\right)e^{im\varphi_k}. \tag{18}$$

Here $\mathbf{k}_\perp = k_\perp(\cos \varphi_k, \sin \varphi_k)$, $\nu = (n_\xi, m)$ enumerates ionization channels identified by parabolic quantum numbers $n_\xi = 0, 1, \ldots$ and $m = 0, \pm 1, \ldots$, and

$$\phi_\nu^{(0)}(\xi) = \varkappa^{1/2}(\varkappa\xi)^{|m|/2}e^{-\varkappa\xi/2}\sqrt{\frac{n_\xi!}{(n_\xi + |m|)!}}L_{n_\xi}^{(|m|)}(\varkappa\xi), \tag{19}$$

where $L_n^{(\alpha)}(x)$ are the generalized Laguerre polynomials [62]. The partial ionization amplitudes $f_\nu(\beta)$ in Eq. (18) are given by [61]

$$f_\nu(\beta) = \frac{\varkappa^{1/2}g_\nu(\beta)}{2^{1/2}}\left(\frac{4\varkappa^2}{F}\right)^{\beta_\nu^{(0)}/\varkappa}$$

$$\times \exp\left[\frac{i\pi}{4} + \frac{i\pi\beta_\nu^{(0)}}{\varkappa} - \varkappa\mu\cos\beta - \frac{\varkappa^3}{3F}\right], \tag{20}$$

where $g_\nu(\beta)$ are the asymptotic coefficients characterizing the initial state (we discuss them below), $\beta_\nu^{(0)} = Z - \varkappa[n_\xi + (|m| + 1)/2]$, $Z = -rV(\mathbf{r})|_{r\to\infty}$ is the Coulomb charge in the asymptotic tail of the potential, and $\mu = -\langle\phi_0|z|\phi_0\rangle$ is the dipole moment in the initial state. For $|z'| \to \infty$, the integral in Eq. (16) can be calculated using the saddle-point method. We thus obtain

$$\phi(\mathbf{r}; \mathbf{F})|_{z'\to-\infty} = \frac{g(z', 0)}{|2\pi z'|^{1/2}} \exp\left[\frac{iF^{1/2}r_\perp'^2}{2|2z'|^{1/2}}\right]$$

$$\times \sum_\nu f_\nu(\beta)\phi_\nu^{(0)}\left(\frac{r_\perp'^2}{2|z'|}\right)e^{im\varphi'}, \tag{21}$$

where $\mathbf{r}'_{\perp} = r'_{\perp}(\cos\varphi', \sin\varphi')$. This asymptotics holds in the region $r'_{\perp} = O(|z'|^{1/2})$. The transverse structure of the ionization flux is described by the sum factor in Eq. (21). Let us discuss it in more detail.

The relative role of the different channels in the sum is determined by the dependence of $f_{\nu}(\beta)$ on F and β. First, we note that the exponential factor in Eq. (20) has the same absolute value for all channels, while the preexponential factor depends on F as $F^{n_{\xi}+(|m|+1)/2}$. Thus in the weak-field case channels with $n_{\xi} > 0$ are suppressed compared to the one with $n_{\xi} = 0$ for the same m, and we neglect their contributions. Consider channels $\nu = (0, m)$ with different m. On the one hand, the preexponential factor in Eq. (20) decreases as $|m|$ grows, so it is sufficient to retain only channels with the smallest $|m|$ present in the sum. On the other hand, only a few channels survive in the sum at small β. Indeed, the difference in the dependence on β originates from the asymptotic coefficient $g_{0m}(\beta)$. At $\beta = 0$, because of the symmetry of the initial state, see Eq. (8), only one coefficient with $m = M$ differs from zero. At small β, coefficients with $m \neq M$ become nonzero, but their distribution in m still peaks at $m = M$. Let us analyze this behavior by deriving $g_{0M\pm1}(\beta)$.

Since the asymptotic coefficients $g_{0m}(\beta)$ are a property of the initial state and their dependence on β is caused by the rotation of the coordinate frame $(x, y, z) \rightarrow (x', y', z')$, it is convenient to use the asymptotic form of $\phi_0(\mathbf{r})$ in spherical coordinates. In the laboratory frame we have

$$\phi_0(\mathbf{r})|_{r\rightarrow\infty} = r^{Z/\varkappa-1}e^{-\varkappa r}\sum_{l=M}^{\infty}C_l Y_{lM}(\theta, \varphi). \quad (22)$$

The coefficient $g_{0M}(0)$ is given in terms of the coefficients C_l by [61]

$$g_{0M}(0) = \frac{2^{1-Z/\varkappa}}{\sqrt{\varkappa^{M+1}M!}}\sum_{l=M}^{\infty}(-1)^l C_l Q(l, M), \quad (23)$$

where

$$Q(l, m) = (-1)^{(|m|-m)/2}\sqrt{\frac{(2l+1)(l+|m|)!}{2(l-|m|)!}}. \quad (24)$$

The rotation of Eq. (22) by an angle β about the y axis can be performed in the standard way using Wigner rotation matrices [63]. However, being interested only in small β, it is easier to develop the expansion in β using the explicit relation $Y_{lm}(\theta, \varphi) = e^{i\beta\hat{l}_y}Y_{lm}(\theta', \varphi')$. In the first order we obtain

$$Y_{lm}(\theta, \varphi) = Y_{lm}(\theta', \varphi') + \frac{\beta}{2}R(l, m)Y_{lm+1}(\theta', \varphi')$$

$$- \frac{\beta}{2}R(l, -m)Y_{lm-1}(\theta', \varphi') + O(\beta^2), \quad (25)$$

where $R(l, m) = \sqrt{(l-m)(l+m+1)}$. Substituting this into Eq. (22) and proceeding as in the derivation of Eq. (23) in [61], for the leading-order channel $m = M$ we obtain

$$g_{0M}(\beta) = g_{0M}(0) + O(\beta^2). \quad (26)$$

For the next to the leading-order channels $m = M \pm 1$ we find

$$g_{0M\pm1}(\beta) = \frac{\pm2^{-Z/\varkappa}\beta}{\sqrt{\varkappa^{M\pm1+1}(M\pm1)!}}\sum_{l=M}^{\infty}(-1)^l R(l, \pm M)$$

$$\times C_l Q(l, M\pm1) + O(\beta^3). \quad (27)$$

This shows that $g_{0M\pm1}(\beta) = O(\beta^1)$. By retaining higher-order terms in Eq. (25), it can be shown that $g_{0m}(\beta) = O(\beta^{|m-M|})$. Thus, indeed, $g_{0m}(\beta)$ quickly decay as $|m - M|$ grows.

Summarizing the discussion, at small β it is sufficient to retain in Eq. (21) only one channel $\nu = (0, M)$ with $f_{0M}(\beta)$ substituted by $f_{0M} = f_{0M}(0)$. The result is

$$\phi(\mathbf{r}; \mathbf{F})|_{z'\rightarrow-\infty} = \frac{-iA_M(F)}{2\pi}\frac{F^{1/2}g(z', 0)}{|2z'|^{1/2}}\left(\frac{Fr'^2_{\perp}}{2|z'|}\right)^{M/2}$$

$$\times \exp\left[\frac{iF^{1/2}r'^2_{\perp}}{2|2z'|^{1/2}} - \frac{\varkappa r'^2_{\perp}}{4|z'|}\right]e^{iM\varphi'}, \quad (28)$$

where

$$A_M(F) = \left.\frac{e^{-iM\varphi_k}A(\mathbf{k}_{\perp}; 0)}{k^M_{\perp}}\right|_{k_{\perp}\rightarrow 0} = \frac{2i\pi^{1/2}f_{0M}}{\sqrt{M!}}\left(\frac{\varkappa}{F}\right)^{(M+1)/2}. \quad (29)$$

The function (28) describes a flux of electrons liberated from the target and moving in the direction $z' \rightarrow -\infty$ opposite to that of $\mathbf{F}$. The first term in the exponent accounts for the fact that the wave front of the flux has a parabolic shape [61], which leads to the appearance of an outgoing radial flux in the plane (x', y'). The second term in the exponent defines the envelope of the flux in the transverse direction. The factor $r'^M_{\perp}e^{iM\varphi'}$ defines the transverse structure of the ionization flux and is of main interest here. One can see that for $M = 0$ the liberated electrons are described by a locally plane wave near the maximum of the envelope at $r'_{\perp} = 0$. But for $M > 0$ they are in a vortex state. This is obvious for $\beta = 0$, which corresponds to the linear polarization case considered in Ref. [28]. The present analysis shows that this also holds for small nonzero β in the case of elliptic polarization.

IV. PROPAGATION

As an electron is liberated from the target, its further motion until rescattering is driven by the field. Since the pioneering paper by Keldysh [64], this propagation stage of the strong-field ionization dynamics is described by Volkov states [65]. In this section we generalize Volkov states to the case of vortex electrons and obtain the electron wave packet arriving for rescattering at the end of propagation.

A. Vortex Volkov states

Is is helpful to preface the analysis of propagation in the present problem by a general discussion of Volkov states. In the context of nonrelativistic strong-field physics, Volkov states are defined as solutions to Eq. (1) with the potential energy term omitted,

$$i\frac{\partial\Phi(\mathbf{r}, t)}{\partial t} = \left[-\frac{1}{2}\Delta + \mathbf{F}(t)\mathbf{r}\right]\Phi(\mathbf{r}, t). \quad (30)$$

In this section we consider an arbitrary field not restricted by Eq. (9). The different solutions to Eq. (30) are specified by the initial condition at $t = t_i$. We are interested in a class of the solutions representing vortex electrons.

The quantum dynamics of an electron in a homogeneous arbitrarily time-dependent electric field can be exactly described in purely classical terms [66]. Let us introduce a

reference classical trajectory with the velocity $\mathbf{v}(t)$ and coordinate $\mathbf{r}(t)$ defined by

$$\dot{\mathbf{v}}(t) = -\mathbf{F}(t), \quad \dot{\mathbf{r}}(t) = \mathbf{v}(t), \tag{31a}$$

$$\mathbf{v}(t \to -\infty) = \mathbf{0}, \quad \mathbf{r}(t \to -\infty) = \mathbf{0}. \tag{31b}$$

All the classical quantities needed for solving Eq. (30) can be expressed in terms of this trajectory. Indeed, the evolution operator $\hat{U}(t, t_i)$ which propagates the solutions from t_i to t is given by

$$\hat{U}(t, t_i) = e^{i\mathcal{S}(\mathbf{r},t)} e^{-i\hat{\mathbf{p}}\mathbf{q}(t) - i\hat{\mathbf{p}}^2(t - t_i)/2}. \tag{32}$$

Here $\hat{\mathbf{p}} = -i\nabla$, $\mathbf{q}(t)$ is the trajectory satisfying Eq. (31a) with the initial conditions $\dot{\mathbf{q}}(t_i) = \mathbf{q}(t_i) = \mathbf{0}$ given explicitly by

$$\mathbf{q}(t) = \mathbf{r}(t) - \mathbf{r}(t_i) - \mathbf{v}(t_i)(t - t_i), \tag{33}$$

and

$$\mathcal{S}(\mathbf{r}, t) = [\mathbf{v}(t) - \mathbf{v}(t_i)]\mathbf{r} - \frac{1}{2} \int_{t_i}^{t} [\mathbf{v}(t') - \mathbf{v}(t_i)]^2 dt' \tag{34}$$

is the classical action accumulated along a trajectory shifted with respect to $\mathbf{q}(t)$ in such a way that at time t it passes through the point $\mathbf{r}$. It can be easily checked that the operator (32) satisfies Eq. (30) with the initial condition $\hat{U}(t_i, t_i) = 1$.

One class of Volkov states is specified by $\Phi(\mathbf{r}, t_i) = e^{i\mathbf{u}\mathbf{r}}$. Using Eq. (32), we obtain

$$\Phi_{\mathbf{u}}(\mathbf{r}, t) = \exp\left[i\mathbf{u}_f(t, t_i, \mathbf{u})\mathbf{r} - \frac{i}{2} \int_{t_i}^{t} \mathbf{u}_f^2(t', t_i, \mathbf{u}) \, dt' \right], \tag{35}$$

where $\mathbf{u}_f(t, t_i, \mathbf{u}) = \mathbf{v}(t) - \mathbf{v}(t_i) + \mathbf{u}$ is the final velocity at time t for the trajectory that begins at time t_i with velocity $\mathbf{u}$. At each $t > t_i$, function (35) is a plane wave whose momentum varies with time and the phase varies accordingly. Such Volkov states are commonly used in strong-field physics.

Consider another class of Volkov states satisfying

$$\Phi(\mathbf{r}, t_i) = J_m(u_\perp r_\perp) e^{im\varphi} e^{iu_z z}. \tag{36}$$

This function describes a vortex state of a free electron, with the vortex axis coinciding with the z axis. The vortex is characterized by the projection of the angular momentum on its axis m, transverse momentum $u_\perp$, and longitudinal momentum u_z. Applying the operator (32) and taking into account that $\hat{\mathbf{p}}^2 \Phi(\mathbf{r}, t_i) = \mathbf{u}^2 \Phi(\mathbf{r}, t_i)$, where $\mathbf{u}^2 = u_\perp^2 + u_z^2$, we obtain

$$\Phi_{m u_\perp u_z}(\mathbf{r}, t) = e^{i\mathcal{S}(\mathbf{r},t) - i\mathbf{u}^2(t - t_i)/2} J_m(u_\perp R_\perp) e^{im\Phi} e^{iu_z Z}. \tag{37}$$

Here

$$\mathbf{R} = \mathbf{r} - \mathbf{q}(t) \tag{38}$$

is the electron coordinate measured relative to $\mathbf{q}(t)$ decomposed in the form $\mathbf{R} = \mathbf{R}_\perp + Z\mathbf{e}_z$, where $\mathbf{R}_\perp = R_\perp(\cos\Phi, \sin\Phi)$ and Z are its components perpendicular and parallel to the z axis, respectively. At each $t > t_i$, function (37) presents a vortex. The quantum number m of the vortex is conserved in time. The vortex axis defined by $R_\perp = 0$ remains parallel to the z axis, but is shifted in the transverse direction by $\mathbf{q}_\perp(t)$, that is, it crosses the (x, y) plane at $\mathbf{r}_\perp = \mathbf{q}_\perp(t)$. We find it remarkable that the axis is not deformed or tilted, only shifted, which is not evident *a priori*. The shift originates from

the transverse component of the field $\mathbf{F}(t)$ and does not appear if the field is linearly polarized along the vortex axis. We call the solutions to Eq. (30) given by Eq. (37) vortex Volkov states. Near the vortex axis, the initial state (36) behaves as $r_\perp^{|m|} e^{im\varphi}$, which complies with the vortex factor in Eq. (28). In Eq. (37), the vortex axis is shifted by $\mathbf{q}_\perp(t)$ and the vortex factor becomes $R_\perp^{|m|} e^{im\Phi}$. This shows what happens with a vortex as it propagates in a laser field. Vortex Volkov states of a relativistic electron obtained by solving the Dirac equation were constructed in Ref. [40].

B. From ionization to rescattering

We now turn to the discussion of propagation between the ionization and rescattering events in the present problem. As a result of tunneling, the target continuously emits a flux of electrons described by Eq. (28) in the direction opposite to that of the instantaneous field $\mathbf{F}(t)$. A part of this flux returns to the target and undergoes rescattering. The goal of this section is to derive the wave packet arriving for rescattering.

This can be done using Green's formula

$$\psi(\mathbf{r}, t) = \frac{1}{2} \int_{-\infty}^{t} dt' \int_{\Sigma'} [G(\mathbf{r}, t; \mathbf{r}', t') \nabla' \psi(t', \mathbf{r}')$$
$$- \psi(t', \mathbf{r}') \nabla' G(\mathbf{r}, t; \mathbf{r}', t')] d\mathbf{\Sigma}', \tag{39}$$

where $\psi(t, \mathbf{r})$ is the solution to Eq. (1) and $G(\mathbf{r}, t; \mathbf{r}', t')$ is the retarded Green's function for Eq. (30) given by [66]

$$G(\mathbf{r}, t; \mathbf{r}', t') = \frac{e^{3i\pi/4}\theta(t - t')}{[2\pi(t - t')]^{3/2}} e^{i\mathcal{S}(\mathbf{r},t;\mathbf{r}',t')}, \tag{40}$$

where [21]

$$\mathcal{S}(\mathbf{r}, t; \mathbf{r}', t') = \mathbf{v}(t)\mathbf{r} - \mathbf{v}(t')\mathbf{r}' + \frac{[\mathbf{r}(t) - \mathbf{r}(t') - \Delta\mathbf{r}]^2}{2(t - t')}$$
$$- \frac{1}{2} \int_{t'}^{t} \mathbf{v}^2(t'') \, dt'' \tag{41}$$

is the classical action accumulated along a trajectory connecting space-time points $(\mathbf{r}', t')$ and $(\mathbf{r}, t)$ and $\Delta\mathbf{r} = \mathbf{r} - \mathbf{r}'$. The spatial integration in Eq. (39) goes over $\mathbf{r}' \in \Sigma'$, where Σ' is a surface enclosing the region beyond which the target potential can be neglected, $d\mathbf{\Sigma}' = \mathbf{n}' d\Sigma'$, $\mathbf{n}'$ is the external unit normal vector to Σ', and $\mathbf{r}$ lies outside Σ'. Equation (39) is obtained by subtracting the equation for $\psi(\mathbf{r}', t')$ multiplied by $G(\mathbf{r}, t; \mathbf{r}', t')$ from the equation for $G(\mathbf{r}, t; \mathbf{r}', t')$ as a function of $\mathbf{r}'$ and t' multiplied by $\psi(\mathbf{r}', t')$ and integrating over t' and $\mathbf{r}'$ lying outside Σ'. It expresses the wave function $\psi(\mathbf{r}, t)$ at time t outside the surface Σ' in terms of its values at all previous times $t' < t$ on the surface Σ'.

We substitute the adiabatic part of the wave function (11) for $\psi(t', \mathbf{r}')$ into the right-hand side of Eq. (39). Following Ref. [21], the result on the left-hand side is denoted by $\psi_r^{(a)}(\mathbf{r}, t)$; in the next section we show that this function gives an incident wave packet from which the rescattering part in Eq. (6) emerges. The derivation is similar to that of Eq. (94) in Ref. [21], so we only outline its main steps omitting the details. We begin by calculating the surface integral in Eq. (39). At a given t', we introduce a rotated coordinate frame $(x', y' = y, z')$ with the z' axis directed along $\mathbf{F}(t')$, as discussed in Sec. III. Then the asymptotics of the SS in Eq. (11)

is given by Eq. (28). The surface integral is accumulated near the direction $z' \to -\infty$, where Σ' crosses the outgoing flux in Eq. (28). We choose Σ' in this region to coincide with a plane $z' = \text{const}$ perpendicular to $\mathbf{F}(t')$ and such that $|z'| \gg a$, where a is the range of the potential; the latter condition is needed for the applicability of Eq. (28). Then $d\mathbf{\Sigma}' = -\mathbf{e}_{z'}d\mathbf{r}'_\perp$ and the surface integral over $\mathbf{r}'_\perp = (x', y')$ can be calculated analytically. The remaining integral over t' is calculated using the saddle-point method. The phase of the integrand is a sum of the classical action $\mathcal{S}(\mathbf{r}, t; z'\mathbf{e}_{z'}, t')$ remaining in Eq. (40) after integration over $\mathbf{r}'_\perp$ and the quantum action $-s(t)$ from Eq. (11). We recall that in the adiabatic regime (5) all classical quantities scale as some powers of ϵ [21]. In particular, the velocity and coordinate for the reference trajectory scale as $v(t) = O(\epsilon^{-1})$ and $r(t) = O(\epsilon^{-2})$. The action (41) scales as $O(\epsilon^{-3})$; this justifies the application of the saddle-point method to the time integral in Eq. (39) and determines the order of the phase of the rescattering part in Eq. (6). The result of the integration over t' depends on the value of r. The requirement that $\mathbf{r}$ must be located outside Σ' leads to the condition $r \gg a = O(\epsilon^0)$. At the same time, being interested in the form of the wave packet returning for rescattering, we want to obtain $\psi_r^{(a)}(\mathbf{r}, t)$ near the target. To fulfill both conditions we consider the region $r = O(\epsilon^0)$. Note that this region belongs to the quasistationary zone where Eq. (6) holds. Let us present the field in the form $\mathbf{F}(t) = F(t)\mathbf{e}(t)$, where $F(t) > 0$ is the field strength and $\mathbf{e}(t)$ denotes a unit polarization vector. Then in the leading order in ϵ the result of the integration is determined by the behavior of the phase of the integrand near a reference point defined by

$$\mathbf{e}(t')\mathbf{u}_i(t, t') = 0 \to t' = t_i(t), \quad (42\text{a})$$

$$u_{i\perp}(t, t_i(t)) = O(\epsilon^1), \quad (42\text{b})$$

where

$$\mathbf{u}_i(t, t') = \mathbf{v}(t') - \frac{\mathbf{r}(t) - \mathbf{r}(t')}{t - t'} \quad (43)$$

is the initial velocity for a closed rescattering trajectory beginning at time t' and returning to the initial point at time t [21]. Equation (42a) may have several solutions, depending on the shape of the pulse. The solutions are times at which ionization should occur for the rescattering to occur at a given time t. In the adiabatic regime the propagation time $t - t_i(t)$ as well as the intervals between the different ionization times $t_i(t)$ scale as $O(\epsilon^{-1})$. Near each $t_i(t)$, there exist two saddle points lying at a distance $O(\epsilon^0)$ from $t_i(t)$, but only one of them contributes to the integral. After evaluating its contribution and calculating the derivatives in Eq. (39) using $\mathbf{e}_{z'}\nabla' = \partial/\partial z'$ the dependence on z' disappears. The result is

$$\psi_r^{(a)}(\mathbf{r}, t) = \frac{-i}{2\pi} \sum_i \frac{A_M(t_i)R'^M_\perp e^{iM\Phi'}e^{i\mathcal{S}(\mathbf{r},t)-is(t_i)}}{(t - t_i)^{3/2+M}F^{1/2}(t_i)}. \quad (44)$$

Here $A_M(t) = A_M(F(t))$, see Eq. (29), $\mathbf{R}$ is the shifted electron coordinate (38), $\mathbf{R}'_\perp = R'_\perp(\cos\Phi', \sin\Phi')$ is its component perpendicular to $\mathbf{e}(t_i)$, one should substitute $t_i = t_i(t)$ throughout, including Eqs. (33) and (34), which makes $R'_\perp$, Φ', and $\mathcal{S}(\mathbf{r}, t)$ implicitly dependent on i, and the summation runs over the different solutions to Eq. (42a). Each term in the sum has the form of a vortex Volkov state, Eq. (37), with the

vortex factor $R'^M_\perp e^{iM\Phi'}$, the action $\mathcal{S}(\mathbf{r}, t)$, and the other factors defining the amplitude of the state. From Eq. (42a) we have $\mathbf{e}(t_i)\mathbf{q}(t) = 0$, which means that, for a given i, the vector $\mathbf{q}(t)$ lies in the plane passing through the origin and perpendicular to $\mathbf{e}(t_i)$. The vortex axis is parallel to $\mathbf{e}(t_i)$ and crosses this plane at $\mathbf{q}(t)$. The longitudinal momentum u_z in Eq. (37) is zero in the present case, because of Eq. (42a). According to Eq. (42b), the transverse momentum $u_\perp$ is $O(\epsilon^1)$. The condition (42b) ensures that the vortex axis is shifted from the origin by $q(t) = O(\epsilon^0)$, and hence $R'_\perp = O(\epsilon^0)$. In this case the argument of the Bessel function in Eq. (37) is $O(\epsilon^1)$ and this function can be replaced by the first term of its expansion near zero, as in Eq. (44).

We are interested in the situation where the vortex axis passes through the region occupied by the target potential, that is, where rescattering of a vortex electron by the target occurs. For this to be the case, the vortex axis should be shifted not too far from the origin, namely, we should have $q(t) = O(\epsilon^0)$. As seen from the above discussion, this holds under the condition (42b). In the general case of elliptically polarized pulses with arbitrary ellipticity this condition can be satisfied only at isolated values of t. The significance of the requirement (10) in the present analysis is explained by the fact that for pulses with such a small ellipticity the condition (42b) is satisfied at all times t, and therefore vortex rescattering is occurring continuously. In this case Eq. (44) can be further simplified. First, we neglect the difference between the directions of $\mathbf{e}(t_i)$ and the laboratory z axis and replace $R'_\perp$ and Φ' by $R_\perp$ and Φ defined by the component $\mathbf{R}_\perp = R_\perp(\cos\Phi, \sin\Phi)$ of $\mathbf{R}$ perpendicular to the laboratory z axis, which incurs an error $O(\epsilon^2)$ in the vortex factor. Second, we neglect the transverse with respect to the z axis component of the reference velocity in Eq. (34), whose contribution to the action is $O(\epsilon^1)$. Then Eq. (44) takes the form

$$\psi_r^{(a)}(\mathbf{r}, t) = \frac{-i}{2\pi} \sum_i \frac{A_M(t_i)R^M_\perp e^{iM\Phi}e^{iu_f(t)z+i\mathcal{S}(t)-is(t_i)}}{(t - t_i)^{3/2+M}|F_z(t_i)|^{1/2}}, \quad (45)$$

where

$$u_f(t) = v_z(t) - v_z(t_i(t)) \quad (46)$$

and

$$\mathcal{S}(t) = -\frac{1}{2}\int_{t_i(t)}^t [v_z(t') - v_z(t_i(t))]^2 dt'. \quad (47)$$

Equation (45) describes the electron wave packet returning for rescattering. Each term in the sum is a vortex moving with velocity $u_f(t)$ along the z axis. The vortex axis is parallel to the z axis and crosses the (x, y) plane at $\mathbf{r}_\perp = \mathbf{q}_\perp(t)$, which plays the role of the impact parameter for the vortex-target collision. The appearance of a nonzero impact parameter is a feature that differs the present analysis from the case of linear polarization considered in Ref. [28]. The impact parameter $q_\perp(t) = O(\epsilon^0)$ varies with time and is controlled by the transverse component of the laser field (9). If $q_\perp(t)$ turns to zero, then $\mathbf{R}_\perp = \mathbf{r}_\perp$ and the corresponding term in Eq. (45) presents an incident vortex wave for a head-on collision, as in Ref. [28]. If $q_\perp(t)$ becomes much larger than the range of the target potential, then $\mathbf{R}_\perp \approx \mathbf{q}_\perp(t)$ and the corresponding term reduces to an incident plane wave, as in Ref. [21].

V. RESCATTERING

As a liberated electron returns to the target, it undergoes rescattering. Equation (45) gives an incident vortex wave packet arriving for rescattering. In this section we introduce vortex scattering states needed to describe the rescattering process and obtain the rescattering parts of the wave function in Eq. (6) and ionization amplitude in Eq. (7).

A. Vortex scattering states

Scattering states in the present axially symmetric potential are defined by the stationary Schrödinger equation

$$\left[-\tfrac{1}{2}\Delta + V(r_\perp, z) - \tfrac{1}{2}k^2\right]\phi(\mathbf{r}) = 0 \qquad (48)$$

supplemented by appropriate asymptotic boundary conditions. Standard textbooks on scattering theory [58] treat only states which take the form of an incident plane wave in the asymptotic region. In recent years, due to the growing interest in vortex electrons and their behavior in various physical processes, a great progress in extending scattering theory to incident vortex waves of different forms has occurred, see a review [38] and references therein. In particular, in Ref. [28] vortex scattering states with the vortex axis coinciding with the symmetry axis of the potential, which corresponds to a head-on vortex-target collision, and zero transverse momentum, which is specific to rescattering in strong-field physics, were introduced. These states satisfy Eq. (48) with the boundary condition

$$\phi_m(\mathbf{r}; k)|_{r\to\infty}$$

$$= \left[(kr_\perp)^{|m|} e^{ikz - i\gamma \ln k(r-z)} + f_m(k, \theta) \frac{e^{ikr + i\gamma \ln 2kr}}{r}\right] e^{im\varphi}, \qquad (49)$$

where $\gamma = Z/k$ and $f_m(k, \theta)$ is the head-on vortex scattering amplitude. For $m = 0$, the first term in Eq. (49) reduces to an incident plane wave, so $f_0(k, \theta)$ coincides with the usual scattering amplitude $f(k, \theta)$ [57,58]. We show in the Appendix that for spherically symmetric potentials $f_m(k, \theta)$ can be expressed in terms of $f(k, \theta)$. Here we generalize these states to the case of a nonzero impact parameter, which is needed for the present problem.

Let $\mathbf{b} = (b_x, b_y) = b(\cos\varphi_b, \sin\varphi_b)$ be a vector lying in the (x, y) plane. We introduce scattering states satisfying

$$\phi_m(\mathbf{r}; k, \mathbf{b})|_{r\to\infty} = (kR_\perp)^{|m|} e^{im\Phi} e^{ikz - i\gamma \ln k(r-z)}$$

$$+ f_m(k, \Omega, \mathbf{b}) \frac{e^{ikr + i\gamma \ln 2kr}}{r}, \qquad (50)$$

where $k > 0$, $\mathbf{R}_\perp = \mathbf{r}_\perp - \mathbf{b} = R_\perp(\cos\Phi, \sin\Phi)$, $f_m(k, \Omega, \mathbf{b})$ is the corresponding scattering amplitude, and $\Omega = (\theta, \varphi)$ are scattering angles, that is, spherical angles defining the direction of $\mathbf{r}$. The vortex axis in Eq. (50) is shifted by $\mathbf{b}$ perpendicularly to the symmetry axis of the potential, so $\mathbf{b}$ plays the role of the impact parameter. While $\phi_m(\mathbf{r}; k)$ can be constructed relatively easy by separating out the azimuthal angle φ in Eq. (48), in the case of $\phi_m(\mathbf{r}; k, \mathbf{b})$ such separation of variables is not possible. It turns out that $f_m(k, \Omega, \mathbf{b})$ can be expressed in terms of $f_m(k, \theta)$, and hence there is no need to solve Eq. (48) with the boundary condition (50) numerically.

In the general case, the scattering amplitude for a vortex state with a given projection m and *nonzero* impact parameter can be expressed using Gegenbauer's addition theorem for the Bessel functions [67] as an infinite sum of terms involving scattering amplitudes for vortices with the different projections m' and *zero* impact parameter [33,35]. The relation we need here could be obtained from the general formula in the limit of zero transverse momentum. However, this relation can be derived in a much simpler way, which is worth documenting. We can represent the vortex factor in Eq. (50) in the form

$$R_\perp^{|m|} e^{im\Phi} = [(x - b_x) + i\sigma(y - b_y)]^{|m|}$$

$$= \sum_{m'=0}^{|m|} \binom{|m|}{m'} (-b_x - i\sigma b_y)^{|m|-m'} (x + i\sigma y)^{m'}$$

$$= \sum_{m'=0}^{|m|} \binom{|m|}{m'} (-b e^{i\sigma\varphi_b})^{|m|-m'} \times r_\perp^{m'} e^{i\sigma m'\varphi}, \qquad (51)$$

where $\sigma = \text{sgn}(m)$ and $\binom{n}{k}$ are the binomial coefficients [62]. The last factor in Eq. (51) is the vortex factor with respect to the z axis, as in Eq. (49). Thus, we can construct $\phi_m(\mathbf{r}; k, \mathbf{b})$ as a linear combination of $\phi_{m'}(\mathbf{r}; k)$ with the coefficients from Eq. (51). This leads to

$$f_m(k, \Omega, \mathbf{b}) = \sum_{m'=0}^{|m|} \binom{|m|}{m'} (-kb e^{i\sigma\varphi_b})^{|m|-m'} f_{m'}(k, \theta) e^{i\sigma m'\varphi}. \qquad (52)$$

In contrast to the general case [33,35], the sum here includes a finite number of terms. In the limit $b \to 0$ only the term with $m' = |m|$ survives in the sum, thus

$$f_m(k, \Omega, \mathbf{0}) = f_m(k, \theta) e^{im\varphi}, \qquad (53)$$

in agreement with Eq. (49). Equation (52) can be simplified for scattering in the backward direction. At $\theta \to \pi$, amplitudes $f_{m'}(k, \theta)$ turn to zero as $(\pi - \theta)^{m'}$, so only one term with $m' = 0$ survives in the sum, and we obtain

$$f_m(k, \Omega, \mathbf{b})|_{\theta=\pi} = (-kb e^{i\sigma\varphi_b})^{|m|} f(k, \pi). \qquad (54)$$

We note that although vortex scattering states defined by Eq. (50) are a particular case of more general states considered in Ref. [38], only these states are needed to describe rescattering in the adiabatic regime.

In the case of a purely Coulomb potential, $V(r_\perp, z) = -Z/r$, Eqs. (48) and (49) can be solved analytically by separating variables in parabolic coordinates, which gives [28]

$$f_m^{(C)}(k, \theta) = \frac{\Gamma(1 + |m| - i\gamma)}{\Gamma(1 - i\gamma)} [-i\cot(\theta/2)]^{|m|} f^{(C)}(k, \theta), \qquad (55)$$

where $f^{(C)}(k, \theta)$ is the usual Coulomb scattering amplitude for $m = 0$ [57,58]. This formula also follows from the general expression for $f_m(k, \theta)$ in terms of $f(k, \theta)$ for spherically symmetric potentials obtained in the Appendix. It turns out that the sum in Eq. (52) in this case can be presented in the closed form

$$f_m^{(C)}(k, \Omega, \mathbf{b}) = M(-|m|, -|m| + i\gamma, -ikb\tan(\theta/2)e^{i\sigma(\varphi_b - \varphi)})$$

$$\times f_m^{(C)}(k, \theta) e^{im\varphi}, \qquad (56)$$

where $M(a, b, x)$ is a confluent hypergeometric function [62]. Thus, in the case of a Coulomb potential, the scattering amplitude for vortex-target collision with a nonzero impact parameter differs from that with zero impact parameter by the M-function factor in Eq. (56). Note that this function is a polynomial of degree $|m|$ of its third argument. The argument diverges at $\theta = \pi$, but this divergence is canceled by the factor $\cot^{|m|}(\theta/2)$ in Eq. (55), so the result is finite and given by Eq. (54).

B. Rescattering part of the wave function

The rescattering part of the wave function in Eq. (6) satisfies the inhomogeneous integral equation [21]

$$\psi_r(\mathbf{r}, t) = \psi_r^{(a)}(\mathbf{r}, t) + \int_{-\infty}^{t} dt' \int G(\mathbf{r}, t; \mathbf{r}', t') \\ \times V(\mathbf{r}')\psi_r(\mathbf{r}', t')d\mathbf{r}', \tag{57}$$

where the incident wave packet (45) plays the role of the source term. We solve this equation following Ref. [21]. Note that the action (47) is $O(\epsilon^{-3})$, while the other terms in the exponent in Eq. (45) are $O(\epsilon^{-1})$. Thus the factor $e^{iS(t)}$ describes the fastest dependence of $\psi_r^{(a)}(\mathbf{r}, t)$ on t, and $\psi_r(\mathbf{r}, t)$ must contain the same factor. Knowing this, it can be seen that the integral over t' in Eq. (57) is accumulated in the zone $|t' - t| = O(\epsilon^2)$. Indeed, in this zone

$$S(\mathbf{r}, t; \mathbf{r}', t') = \frac{(\mathbf{r} - \mathbf{r}')^2}{2(t - t')} + O(\epsilon^2), \tag{58a}$$

$$S(t') = S(t) + \tfrac{1}{2}u_f^2(t)(t - t') + O(\epsilon^2), \tag{58b}$$

where $u_f(t)$ is the incident velocity of the wave packet given by Eq. (46). The fact that $u_f(t) = O(\epsilon^{-1})$ confirms the above statement. Equation (58a) means that the function (40) reduces to the retarded Green's function for a free electron. Equation (58b) shows that the integral term in Eq. (57) is proportional to $e^{iS(t)}$, so this factor can be canceled from the equation. Upon substituting Eqs. (58) into Eq. (57) the integration over t' Fourier transforms G into the outgoing-wave Green's function for a free electron at the collision energy $u_f^2(t)/2$. Thus Eq. (57) reduces to the integral equation for a stationary vortex scattering state satisfying Eq. (48) with the asymptotic boundary condition (50), where $m = M$, $k = u_f(t)$, and $\mathbf{b} = \mathbf{q}_\perp(t)$. Omitting further details [21], the solution to Eq. (57) is

$$\psi_r(\mathbf{r}, t) = \frac{-i}{2\pi} \sum_i \frac{A_M(t_i)\phi_M(\mathbf{r}; u_f(t), \mathbf{q}_\perp(t)) \, e^{iS(t) - is(t_i)}}{[u_f(t)(t - t_i)]^M |(t - t_i)^3 F_z(t_i)|^{1/2}}, \tag{59}$$

where $t_i = t_i(t)$ and for simplicity we assumed that $u_f(t) > 0$. This formula gives the adiabatic asymptotics of the rescattering part of the wave function in Eq. (6) for the case of rescattering of vortex electrons generated by elliptically polarized pulses characterized by Eq. (10). Note that in the present case the phase of $\psi_r(\mathbf{r}, t)$ is $O(\epsilon^{-3})$, as in the general case [21], but its amplitude is $O(\epsilon^{3/2+2M})$, which is suppressed by a factor of $O(\epsilon^{2M})$ compared to the general case.

C. Rescattering part of the ionization amplitude

The rescattering part of the ionization amplitude in Eq. (7) is given by [21]

$$I_r(\mathbf{k}) = \frac{-i}{2} \int_{-\infty}^{\infty} dt \int_\Sigma [e^{-iS(\mathbf{r}, t; \mathbf{k})}\nabla\psi_r(\mathbf{r}, t) \\ - \psi_r(\mathbf{r}, t)\nabla e^{-iS(\mathbf{r}, t; \mathbf{k})}]d\boldsymbol{\Sigma}, \tag{60}$$

where the spatial integration goes over a surface Σ enclosing the region occupied by the target potential, $d\boldsymbol{\Sigma} = \mathbf{n}d\Sigma$, and $\mathbf{n}$ is the external unit normal vector to Σ. The action in Eq. (60) is given by

$$S(\mathbf{r}, t; \mathbf{k}) = \mathbf{u}_i(t, \mathbf{k})\mathbf{r} - \frac{1}{2}\int_0^t \mathbf{u}_i^2(t', \mathbf{k})dt', \tag{61}$$

where $\mathbf{u}_i(t, \mathbf{k}) = \mathbf{k} - \mathbf{v}_\infty + \mathbf{v}(t)$ is the initial velocity with which an electron should begin its classical motion at time t to end with a given asymptotic velocity $\mathbf{k}$ and $\mathbf{v}_\infty = \mathbf{v}(t \to \infty)$. We choose Σ to be a sphere of sufficiently large radius r, so that upon substituting Eq. (59) into Eq. (60) the scattering state can be replaced by its asymptotic form given by Eq. (50). The first term in Eq. (50) does not contribute to Eq. (60), so the vorticity of the incident wave does not reveal itself and the integrals can be calculated in the same way as in Ref. [21]. The surface integral is calculated using Eq. (137) from Ref. [21]. The time integral is evaluated using the saddle-point method, the corresponding action is

$$S_r(t, \mathbf{k}) = \frac{1}{2}\int_0^t \mathbf{u}_i^2(t', \mathbf{k})dt' - S(t) - s(t_i). \tag{62}$$

In the leading order in ϵ the result of the integration is determined by the behavior of this function near a reference point defined by

$$\mathbf{u}_i^2(t, \mathbf{k}) = u_f^2(t) \quad \rightarrow \quad t = t_r(\mathbf{k}). \tag{63}$$

The incident velocity of rescattering is $u_f(t)\mathbf{e}_z$, the final velocity after rescattering for a given $\mathbf{k}$ should be $\mathbf{u}_i(t, \mathbf{k})$, thus Eq. (63) ensures the conservation of energy in the rescattering event and this defines the rescattering time $t_r(\mathbf{k})$. Omitting further details, the result is

$$I_r(\mathbf{k}) = \sum_{ir} \frac{e^{i\pi/4}(2\pi)^{1/2}A_M(t_i)e^{iS_r(t_r, \mathbf{k})}}{[u_f(t_r)(t_r - t_i)]^M |(t_r - t_i)^3 F_z(t_i)S_r''|^{1/2}} \\ \times f_M(u_f(t_r), \Omega_i, \mathbf{q}_\perp(t_r)), \tag{64}$$

where

$$S_r'' = F_z(t_r)[u_f(t_r) - u_{iz}(t_r, \mathbf{k})] + \frac{u_f^2(t_r)}{t_r - t_i}. \tag{65}$$

Here $t_i = t_i(t_r(\mathbf{k}))$ and $t_r = t_r(\mathbf{k})$ are the ionization and rescattering times for a given $\mathbf{k}$, $\Omega_i = (\theta_i, \varphi_i)$ are spherical angles defining the direction of $\mathbf{u}_i(t_r, \mathbf{k})$, and the summation runs over the different solutions to Eqs. (42) and (63). Equation (64) generalizes the adiabatic asymptotics of $I_r(\mathbf{k})$ obtained in Ref. [21] to the specific configuration of the present problem. This completes the derivation indicated in the end of Sec. II.

VI. IMAGING

The problem of imaging, that is, extracting target structure information from the observable PEMD, attracts much attention in strong-field physics. A fruitful approach to imaging was proposed in Ref. [3]. It was recognized that in a certain region of the photoelectron momentum space the PEMD is proportional to the DCS for elastic scattering of a photoelectron on the parent ion. The DCS given by the absolute value squared of the corresponding scattering amplitude is the information that can be extracted. The uniform treatment of rescattering developed on the basis of the adiabatic theory [21] in Ref. [22] turned the idea of Ref. [3] into a powerful quantitative method [23–27]. In Ref. [28] this method was generalized to rescattering of vortex electrons generated by linearly polarized pulses. In this case it yields the absolute value squared of the head-on vortex scattering amplitude $f_m(k, \theta)$ defined by Eq. (49). Here we further generalize the method by showing that imaging with vortex electrons generated by elliptically polarized pulses enables one to extract the absolute value squared of the vortex scattering amplitude $f_m(k, \Omega, \mathbf{b})$ with a nonzero impact parameter defined by Eq. (50).

Having constructed the rescattering part of the wave function, Eq. (59), we can extend the theory developed in Ref. [22] to the present configuration. Two main objects appearing in the theory are a backward rescattering caustic and the factorization formula. We begin with the discussion of the caustic. The classical caustic is a surface in the space of photoelectron momenta $\mathbf{k}$ where a pair of long and short backward rescattering trajectories originating from the same half-cycle of the laser field coalesce [68]. It can be defined for the general case of elliptic polarization. However, we restrict our treatment here to small ellipticities satisfying Eq. (10). In this case the caustic approximately coincides with that for a linearly polarized field with the same $F_z(t)$, the difference scales as $O(\epsilon^2)$ and can be neglected in the adiabatic regime (5). We adopt this approximation below. It is convenient to parametrize the caustic by scattering angles $\Omega = (\theta, \varphi)$ characterizing the coalesced trajectories. The ionization t_i and rescattering t_r times at the caustic satisfy [22]

$$u_{iz}(t_r, t_i) = 0, \tag{66a}$$

$$2F_z(t_r) \sin^2(\theta/2) + \frac{u_f(t_r)}{t_r - t_i} = 0. \tag{66b}$$

These equations define functions $t_i(\theta)$ and $t_r(\theta)$, and hence the incident velocity $u_f(\theta) = u_f(t_r(\theta))$ and impact parameter $\mathbf{q}_\perp(\theta) = \mathbf{q}_\perp(t_r(\theta))$ for rescattering at the caustic. In the rest of this section we omit the argument θ of these functions, implying that all the kinematic characteristics of rescattering are taken at the caustic. The classical caustic is a surface of revolution about the k_z axis having the form [22]

$$\mathbf{k}_c(\Omega) = (k_\perp(\theta) \cos \varphi, k_\perp(\theta) \sin \varphi, k_z(\theta)), \tag{67}$$

where

$$k_\perp(\theta) = |u_f| \sin \theta, \tag{68a}$$

$$k_z(\theta) = u_f \cos \theta + v_\infty - v_z(t_r). \tag{68b}$$

In arriving at Eq. (64) the integral over time in Eq. (60) was calculated using the saddle-point method. Each saddle point is associated with a rescattering trajectory satisfying Eqs. (42) and (63). The coalescence of two such trajectories at a classical caustic results in the coalescence of two saddle points at the corresponding quantum caustic. The difference between the two caustics is caused by a quantum term $s(t_i)$ in the action (62). The quantum caustic is given by

$$\mathbf{k}_q(\Omega) = \mathbf{k}_c(\Omega) + q(\theta)\boldsymbol{\nu}(\Omega), \tag{69}$$

where

$$q(\theta) = \frac{-E(t_i)}{(t_r - t_i)|F_z(t_i)|} \tag{70}$$

and $\boldsymbol{\nu}(\Omega)$ is the external unit normal vector to the surface $\mathbf{k}_c(\Omega)$. The quantum shift (70) between the caustics was observed experimentally [26]. Note that it is generally complex, since the SS energy eigenvalue $E(t)$ is complex. Also note that $q(\theta) = O(\epsilon^1)$, so the caustics merge in the limit (5).

We now turn to the factorization formula. The asymptotics (64) is obtained by calculating individual contributions from each saddle point to the time integral in Eq. (60). However, in the region of the photoelectron momentum space near a caustic the two coalescing saddle points cannot be treated separately. The uniform asymptotics of their collective contribution $I_c(\mathbf{k})$ to $I_r(\mathbf{k})$ in this region can be calculated using Eq. (59) and following Ref. [22]. Consider the outermost caustic either in the positive or negative direction of the k_z axis. In the vicinity of the caustic photoelectron momenta can be presented in the form

$$\mathbf{k} = \mathbf{k}_c(\Omega) + \Delta k \boldsymbol{\nu}(\Omega). \tag{71}$$

Thus the set $(\Omega, \Delta k)$ can be used as curvilinear coordinates near the caustic, with Ω defining the position at the caustic and Δk giving the distance from the caustic along the normal $\boldsymbol{\nu}(\Omega)$ to it. The corresponding $I_c(\mathbf{k})$ is the only contribution to the total ionization amplitude (7) in this region, so the PEMD is given by $P_c(\mathbf{k}) = |I_c(\mathbf{k})|^2$. Omitting further details, we obtain

$$P_c(\mathbf{k}) = \left| f_M\left(u_f, \Omega, \mathbf{q}_\perp\right) \right|^2 W_M(\theta, \Delta k), \tag{72}$$

where

$$W_M(\theta, \Delta k) = |\text{Ai}(\alpha[\Delta k - q(\theta)])|^2 \left| \frac{2}{S_r'''} \right|^{2/3}$$
$$\times \frac{4\pi^2 |A_M(t_i)|^2}{u_f^{2M}(t_r - t_i)^{3+2M}|F_z(t_i)|} \exp\left[-\int_{-\infty}^{t_i} \Gamma(t) \, dt \right]. \tag{73}$$

Here $\text{Ai}(x)$ is the Airy function [62], $\alpha = (2/S_r''')^{1/3}|u_f|$, where the explicit form of S_r''' is given in Ref. [22], $\Gamma(t) = -2\text{Im}[E(t)]$ is the instantaneous ionization rate, and we recall that t_i, t_r, u_f, and $\mathbf{q}_\perp$ are functions of θ taken at the classical caustic. Equation (72) is the factorization formula. It holds in the vicinity of the classical caustic of width $\Delta k = o(\epsilon^{-1})$ [22] including the quantum caustic. Note that at the quantum caustic $\Delta k = q(\theta)$, so the argument of the Airy function in Eq. (73) turns to zero. The factor (73) is called the RWP. Knowing this factor, one can find the first factor in Eq. (72) from a given PEMD, which establishes a method of target

structure imaging. The factorization formula (72) differs from that for vortex electrons in the linear polarization case derived in Ref. [22] only by the scattering amplitude, the RWP (73) remains the same because of the small ellipticity. This difference, however, is essential since it opens a new window for imaging providing a view on the target structure information contained in the amplitude $f_M(u_f, \Omega, \mathbf{q}_\perp)$.

VII. ILLUSTRATIVE RESULTS AND DISCUSSION

To illustrate the theory, we consider ionization from an active π orbital in two atomic systems: a one-electron ion $He^+(2p, m = 1)$ and a many-electron neutral atom $Xe(5p, m = 1)$ treated in the single-active-electron approximation. PEMDs for these systems generated by ionization from initial orbitals with $m = 0$ and 1 in the linear polarization case were compared in Ref. [28]. We recall that the present theory is an asymptotics which applies under the conditions (5) and (10). This means that its predictions converge to the exact results as the adiabatic parameter ϵ tends to zero. The calculations discussed below are done for pulses (9) with frequency $\omega = 0.057$ (wavelength $\lambda = 800$ nm), which corresponds to $\epsilon \sim 0.1$. The good quantitative performance of the adiabatic theory in this case was demonstrated, e.g., in Refs. [21,22,28]. From Eq. (10) we obtain $\varepsilon \sim 0.01$, which determines the range of ellipticities to be treated. We consider pulses with a Gaussian envelope

$$f(t) = -\exp[-(2t/T)^2]. \tag{74}$$

The duration of the pulse T is specified by $\omega T = 2\pi n_{oc}$, where n_{oc} is the number of optical cycles in the pulse. In all the calculations we set $n_{oc} = 2$. In this case the outermost caustic in the region $k_z < 0$ is well separated from other caustics as well as from the region where the adiabatic part of the ionization amplitude (7) dominates, and hence Eq. (72) gives the total PEMD in the vicinity of the caustic [22,28]. The goal of the calculations is to illustrate novel features in the structure of the PEMD near the caustic resulting from vortex rescattering with a nonzero impact parameter. Since these features manifest themselves in the dependence of the PEMD on the scattering angles $\Omega = (\theta, \varphi)$, that is, in its behavior at the caustic, while the dependence on the coordinate Δk normal to the caustic is described by the same universal Airy-function factor in the RWP (73) as in Refs. [22,28], we consider only the behavior of $P_c(\mathbf{k})$ at the quantum caustic.

A. $He^+(2p, m = 1)$

We first discuss ionization from the $2p1$ state of He^+. In this case $Z = 2$, $M = 1$, $E_0 = -0.5$, and $g_{01} = 1$. The scattering amplitudes are calculated using Eqs. (A7), (55), and (56). We begin with a pulse with $F_0 = 0.1$ and $\omega = 0.057$. The sections of the classical and quantum caustics by a half-plane $(k_\perp, k_z)$ calculated for this pulse are shown in Fig. 1. We consider caustics in the interval $90° \leqslant \theta \leqslant 180°$; at smaller θ they enter the region in the photoelectron momentum space where other contributions to the PEMD cannot be neglected [22,28]. The top panel in Fig. 2 shows the incident velocity $u_f(\theta)$ of rescattering at the classical caustic. The sign in Eq. (74) is chosen such that $u_f(\theta) > 0$. For pulses polarized in the (x, z) plane, as in Eq. (9), we have $\mathbf{q}_\perp(\theta) = q_\perp(\theta)\mathbf{e}_x$. The
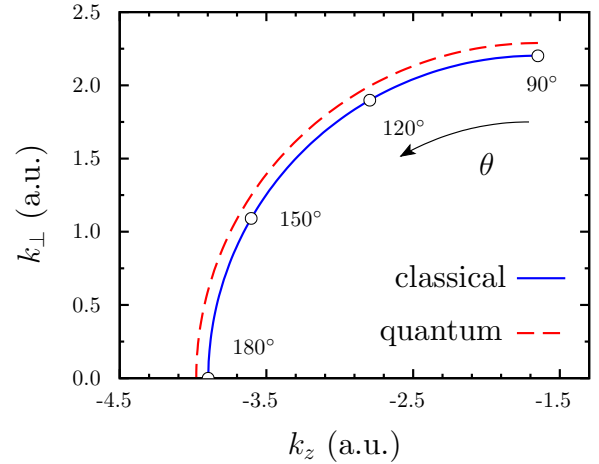
FIG. 1. Solid (blue) and dashed (red) lines show sections of the classical [Eq. (67)] and quantum [Eq. (69)] caustics, respectively, by a half-plane $(k_\perp, k_z)$. The caustics are calculated for a two-cycle pulse with $F_0 = 0.1$ and $\omega = 0.057$. The target-dependent quantum shift (70) between them is calculated for $He^+(2p1)$. The sections of the caustics are parameterized by the scattering angle θ, see Eq. (68).

middle panel shows the impact parameter $q_\perp(\theta)$ calculated with $\varepsilon = 0.0015$. For the present choice of the sign of $F_x(t)$ in Eq. (9) the impact parameter is positive, which corresponds to $\varphi_b = 0$ in Eq. (52). The value of $q_\perp(\theta)$ scales as $\varepsilon/\omega^2 = O(\epsilon^0)$, so even for such a small ellipticity it is of the order of one atomic unit at the frequency considered. Note that both $u_f(\theta)$ and $q_\perp(\theta)$ only slightly vary along the caustic. These
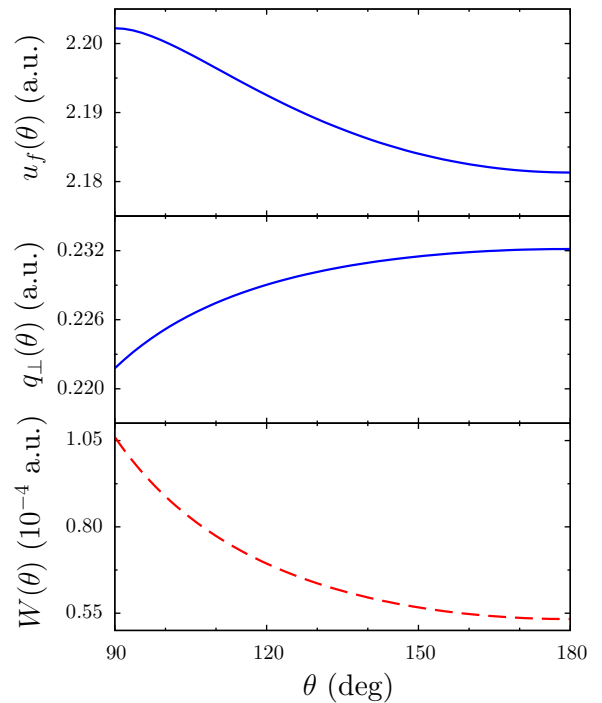
FIG. 2. The incident velocity $u_f(\theta)$ (top) and impact parameter $q_\perp(\theta)$ (middle) for rescattering at the classical caustic and the RWP (73) at the quantum caustic (bottom) as functions of the scattering angle θ calculated for $He^+(2p1)$ interacting with a pulse with $F_0 = 0.1$ and $\omega = 0.057$, as in Fig. 1. The impact parameter is calculated with $\varepsilon = 0.0015$.
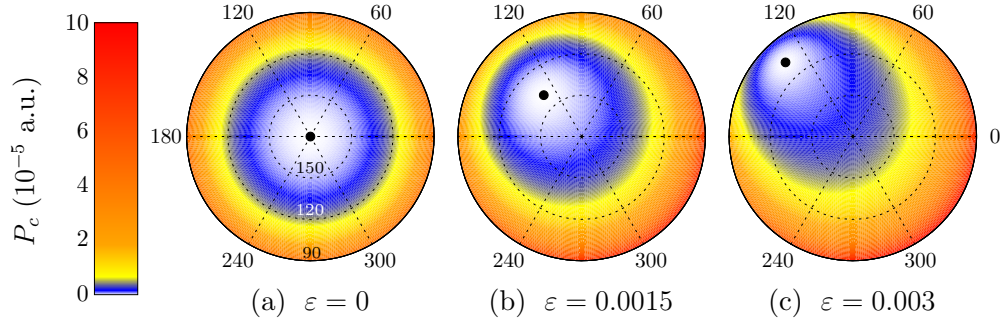
FIG. 3. PEMDs for He$^+(2p1)$ as functions of the scattering angles θ and φ at the quantum caustic calculated using Eq. (72) for three pulses with $F_0 = 0.1$ and $\omega = 0.057$, as in Figs. 1 and 2, and different ellipticities. The radial coordinate in the plots is θ varying from 180° at the center of the circular region to 90° at its boundary. Dashed circles indicate intermediate values $\theta = 150°$ and 120°, as shown in (a). The polar angle is φ; radial dashed lines indicate its values in degrees. The solid black circles indicate the zero of the PEMD.

kinematic quantities are fully determined by the field. The bottom panel in Fig. 2 shows the target-dependent RWP (73) at the quantum caustic. It is a smooth structureless function, which means that all peculiarities in the behavior of the PEMD at the caustic, if any, are caused by the first factor in Eq. (72).

Figure 3 shows PEMDs as functions of the scattering angles θ and φ at the quantum caustic calculated using Eq. (72) for three pulses with the same $F_0 = 0.1$ and $\omega = 0.057$ as in Figs. 1 and 2 and different ellipticities. The plots show the azimuthal equidistant projection (like on the emblem of the United Nations) of the caustic centered at $\theta = 180°$, with the radial coordinate giving the value of $180° - \theta$ (in degrees) and the polar angle equal to φ. For $\varepsilon = 0$, the PEMD is axially symmetric about the k_z axis and does not depend on φ. For $\varepsilon > 0$, it becomes dependent on φ. For the present case of a purely Coulomb potential the behavior of the PEMD at the caustic is rather smooth and simple. The only feature attracting attention is a zero indicated in Fig. 3 by solid black circles. The zero is located at $\theta = 180°$ for $\varepsilon = 0$ and moves to smaller θ in the direction of $\varphi \approx 132°$ as ε grows. Let us discuss this feature in more detail.

The Coulomb scattering amplitude (56) turns to zero at the zeros of the M-function factor. This factor is a polynomial of degree $|m|$, so in the present case it has one zero. The scattering amplitude in Eq. (72) turns to zero under the condition

$$Z + iu_f(\theta) + e^{-i\varphi}\tan(\theta/2)q_\perp(\theta)u_f^2(\theta) = 0. \quad (75)$$

The solution of this complex equation with respect to two real variables θ and φ defines scattering angles θ_0 and φ_0 giving the position of the zero of the PEMD at the caustic. Solid (navy) lines in Fig. 4 show the dependence of θ_0 and φ_0 on ε varying continuously for pulses with the same $F_0 = 0.1$ and $\omega = 0.057$ as in Fig. 3. In the interval of ε considered, θ_0 decreases from 180°–90°, while φ_0 varies very little staying near 132°. To understand this behavior, we recall that $u_f(\theta)$ and $q_\perp(\theta)$ remain almost constant along the caustic, see Fig. 2. Therefore these functions can be replaced in Eq. (75) by their values at $\theta = \pi$, which leads to the approximate solution

$$\theta_0 \approx 2\arctan\frac{\sqrt{Z^2 + u_f^2(\pi)}}{q_\perp(\pi)u_f^2(\pi)}, \quad (76a)$$

$$\varphi_0 \approx \pi - \arctan\frac{u_f(\pi)}{Z}. \quad (76b)$$

We call this the $\theta = \pi$ approximation. Its results are shown by dashed (red) lines in Fig. 4. Taking into account that $q_\perp(\pi) \propto \varepsilon$ while the other quantities in Eq. (76) are independent of ε, these equations explain the behavior seen in Fig. 4.

We next discuss the dependence of θ_0 and φ_0 on the frequency and amplitude of the pulse. Figure 5 illustrates the dependence on ω for three values of F_0 at a fixed ellipticity $\varepsilon = 0.0015$. Both angles are seen to strongly depend on the pulse parameters. They vary in wide ranges in the intervals of ω and F_0 considered which are typical for strong-field physics. This can be used for extracting the pulse parameters, particularly the pulse amplitude F_0, which is usually not known exactly in experiments [26], from the position of the zero of the PEMD. Note that the approximation given by Eq. (76) works very well.

However, of main interest for us is the target structure information that can be extracted from the PEMD. This information is represented by the first factor in Eq. (72). In the case of a purely Coulomb potential the corresponding scattering
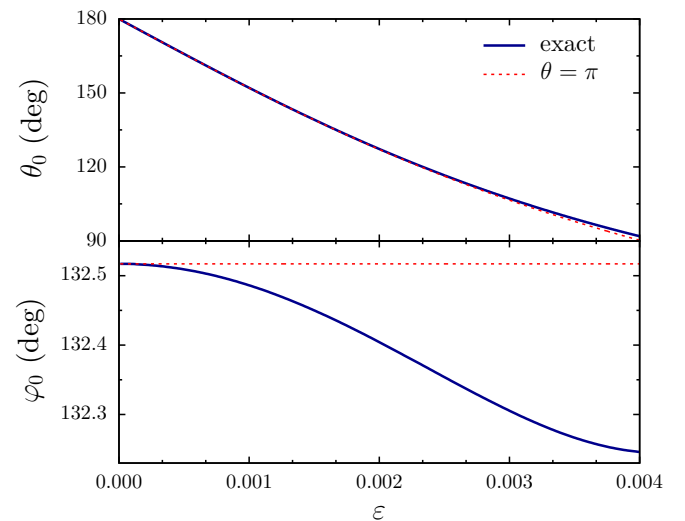
FIG. 4. Scattering angles θ_0 and φ_0 giving the position of the zero of the PEMD for He$^+(2p1)$ as functions of the ellipticity ε for pulses with $F_0 = 0.1$ and $\omega = 0.057$, as in Fig. 3. Solid (navy) lines show the exact results obtained by solving Eq. (75). Dashed (red) lines denoted by $\theta = \pi$ show approximate results from Eq. (76).
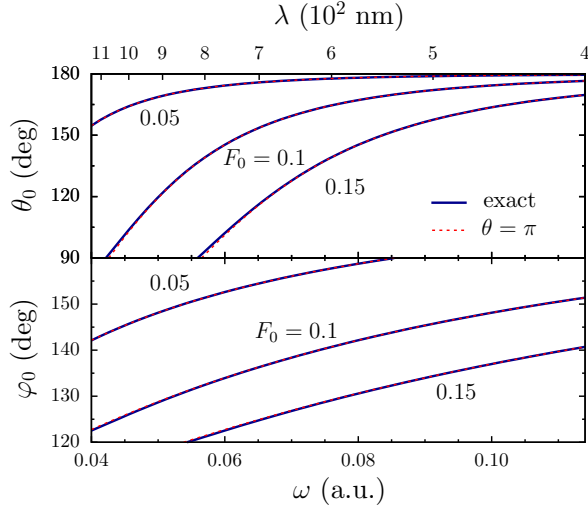
FIG. 5. Similar to Fig. 4, but now θ_0 and φ_0 are shown as functions of pulse frequency ω (the top axis shows the corresponding wavelength λ) calculated for three amplitudes F_0 indicated in the figure at a fixed ellipticity $\varepsilon = 0.0015$. The dashed (red) lines obtained in the $\theta = \pi$ approximation lie on the top of the solid (navy) lines showing the exact results.

amplitude is known analytically, see Eq. (56). We emphasize that this amplitude cannot be measured in the usual collision experiment with a plane-wave front of the incident electron beam. The only parameter characterizing the Coulomb potential is the nuclear charge Z, and in the present model $Z = 2$. As can be seen from Eq. (76), both angles θ_0 and φ_0 strongly depend on Z. This gives an example of how a specific

property of the target is encoded in and can be extracted from the PEMD.

B. Xe($5p, m = 1$)

To illustrate the sensitivity of the behavior of the PEMD at the caustic on the target, we discuss ionization from the $5p1$ orbital in Xe. It should be noted that in the present configuration tunneling ionization from the $5p0$ orbital in Xe dominates. A more realistic target for which predictions of our theory could be observed experimentally is a linear molecule with an active π orbital (like NO) aligned along the major axis of polarization of the laser field. We consider Xe($5p1$) as a simple model for such a molecule. The ionizing $5p1$ orbital in Xe is calculated using a one-electron potential defined in Ref. [69]; the same potential was used in previous calculations [22,28] and in the analysis of experiments [23,26]. In this case $Z = 1$, $M = 1$, $E_0 = -0.446$, and $g_{01} = 3.6$. The scattering amplitudes are calculated using Eqs. (A9), (A10), and (52).

Figure 6 shows PEMDs at the quantum caustic calculated using Eq. (72) for six pulses with $F_0 = 0.1$ and $\omega = 0.057$ and different ellipticities. In the present case the PEMD exhibits a much richer structure. It has a zero similar to the one discussed in the previous subsection. This zero is located in the center of Fig. 6(a) at $\theta = 180°$ for $\varepsilon = 0$ and moves to smaller θ in the direction of $\varphi \approx 270°$ as the ellipticity grows. We note that regions near zeros of the PEMD are shown in Fig. 6 by white color; this color is located below the blue color in color bar scales, but is not seen there. In addition, there exist other zeros, local minima, and maxima and all these structures rapidly vary with the elipticity. The structure of the PEMD can be understood by considering the behavior of
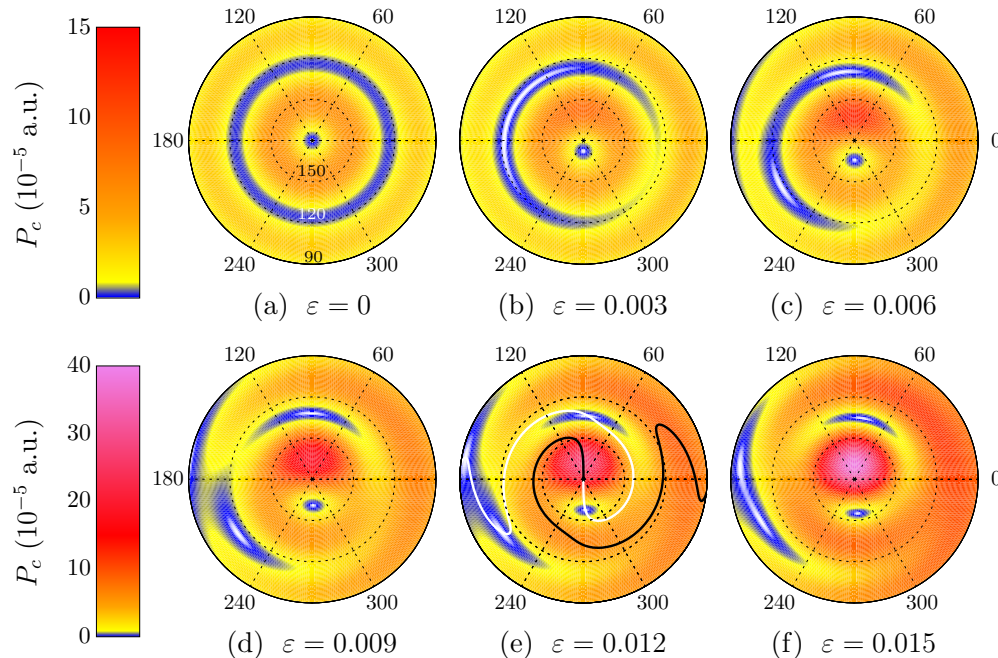
FIG. 6. PEMDs for Xe($5p1$) at the quantum caustic calculated using Eq. (72) for six pulses with $F_0 = 0.1$ and $\omega = 0.057$ and different ellipticities. The coordinates in the plots are related to the scattering angles θ and φ as explained in the caption to Fig. 3. The white and black lines in (e) show angles $\varphi_{\min}$ and $\varphi_{\max}$, see Eq. (78), giving the positions of the minimum and maximum, respectively, of the PEMD as a function of φ at a fixed θ. The imaging procedure applies at these lines.
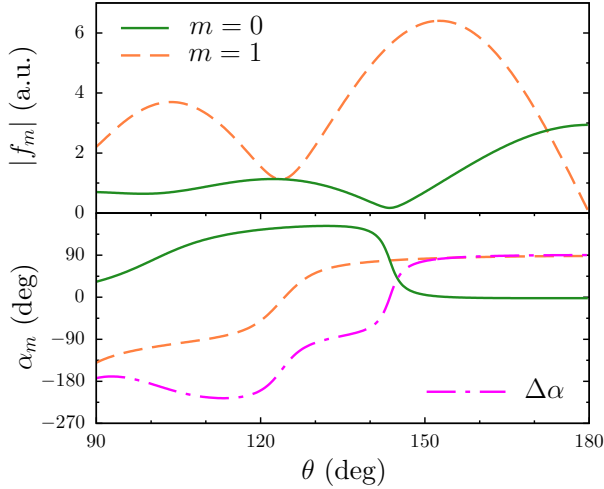
FIG. 7. Absolute values (top) and phases (bottom) of the head-on vortex scattering amplitudes $f_m(u_f(\theta), \theta) = |f_m|e^{i\alpha_m}$ with $m = 0$ (solid green lines) and 1 (dashed orange lines) for the potential modeling $Xe(5p1)$ in the single-active-electron approximation as functions of the scattering angle θ at the caustic. The dash-dotted (magenta) line in the bottom panel shows the phase difference $\Delta\alpha = \alpha_1 - \alpha_0$. The imaging procedure discussed in the text yields the values of $|f_0|$, $|f_1|$, and $\Delta\alpha$.

the head-on vortex scattering amplitudes with $m = 0$ and 1 as functions of θ shown in Fig. 7. For $\varepsilon = 0$, the scattering amplitude in Eq. (72) coincides with the head-on vortex amplitude $f_1(u_f(\theta), \theta)$. The absolute value of this amplitude turns to zero at $\theta = 180°$ and has a pronounced minimum at $\theta \approx 124°$. This minimum is seen as a circular blue ravine in Fig. 6(a). For $\varepsilon > 0$, a nonzero contribution from the plane-wave amplitude $f_0(u_f(\theta), \theta)$ appears in Eq. (52). The interference of the two amplitudes produces the structures seen Fig. 6. As ε grows, the ravine becomes asymmetric and acquires a minimum at $\varphi \approx 158°$, see Fig. 6(b). Then the value of the PEMD at the minimum turns to zero and the zero splits into two zeros, which quickly depart from each other in the φ direction, see Fig. 6(c). Further increase of ε results in the relative motion of these two zeros also in the θ direction and appearance of one more zero at $\varphi \approx 173°$, see Fig. 6(d). In Figs. 6(e) and 6(f) two of the zeros coalesce. The rapid dependence on ε is explained by the fact that in the expression for the scattering amplitude in Eq. (72) following from Eq. (52) the plane-wave amplitude $f_0(u_f(\theta), \theta)$ appears multiplied by the impact parameter $q_\perp(\theta)$ which is proportional to ε. Thus the behavior of the first factor in Eq. (72) at the caustic can be controlled by varying ε.

Let us analyze the interference of the two amplitudes discussed above more quantitatively. Using Eq. (52), the first factor in Eq. (72) at the caustic takes the form

$$|u_f(\theta)q_\perp(\theta)f_0(u_f(\theta), \theta) - f_1(u_f(\theta), \theta)e^{i\varphi}|^2$$
$$= |u_f q_\perp f_0|^2 + |f_1|^2 - 2|u_f q_\perp f_0 f_1|\cos(\Delta\alpha + \varphi). \quad (77)$$

In the second line scattering amplitudes are presented in the form $f_m = |f_m|e^{i\alpha_m}$, were α_m is the phase of f_m, $\Delta\alpha = \alpha_1 - \alpha_0$ is their phase difference, and for brevity we omit arguments of the functions. Equation (77) suggests the following

imaging procedure. Given a calculated or measured PEMD at the caustic for a nonzero ellipticity, it should be considered as a function of φ at a fixed θ. One should find the minimum and maximum of this function. The white and black lines in Fig. 6(e) show their positions $\varphi_{\min}$ and $\varphi_{\max}$, respectively, as functions of θ for the present model. From Eq. (77) we obtain

$$\varphi_{\min} = -\Delta\alpha, \quad \varphi_{\max} = \varphi_{\min} + \pi, \quad (78)$$

where both angles are defined modulo 2π. Thus knowing any one of these angles one can find $\Delta\alpha$. Simultaneously with $\varphi_{\min}$ and $\varphi_{\max}$ one finds the values of the PEMD at the minimum and maximum According to Eqs. (72) and (77), they are given by

$$P_{\min} = (|u_f q_\perp f_0| - |f_1|)^2 W_1,$$
$$P_{\max} = (|u_f q_\perp f_0| + |f_1|)^2 W_1, \quad (79)$$

where W_1 is the RWP (73). Following Refs. [22,28], we assume that the values of u_f and $q_\perp$ determined by the field as well as of W_1, which depends on the target only through the SS energy eigenvalue $E(t)$, are known. Then knowing $P_{\min}$ and $P_{\max}$ one can find the combinations $||u_f q_\perp f_0| - |f_1||$ and $|u_f q_\perp f_0| + |f_1|$. From them, taking into account that f_1 turns to zero at $\theta = \pi$, one can find $|f_0|$ and $|f_1|$. Summarizing, the procedure yields a rich set of target structure information consisting of the absolute values of two head-on vortex scattering amplitudes, $f_0(u_f(\theta), \theta)$ and $f_1(u_f(\theta), \theta)$, and their phase difference $\Delta\alpha(\theta)$ as functions of the scattering angle θ in the interval covered by the PEMD. This is a remarkable result. For comparison, we mention that a similar imaging procedure with plane-wave electrons yields only $|f_0(u_f(\theta), \theta)|$ [22] and that with vortex electrons in the linear polarization case yields $|f_m(u_f(\theta), \theta)|$ for a single m determined by the initial state [28]. The nonzero ellipticity activates the dependence of the PEMD on φ, and through this dependence more information becomes accessible.

We mention that similar reasoning can be applied to imaging using vortex electrons with $M > 1$. Consider $f_M(u_f, \Omega, q_\perp)$ as a function of φ at a fixed θ. Equation (52) gives the Fourier expansion of this function containing exponents $e^{im'\varphi}$ with $m' = 0, \ldots, M$. Substituting Eq. (52) into Eq. (72), one obtains the Fourier expansion of the PEMD containing exponents with $m' = -M, \ldots, M$. On the one hand, the $2M + 1$ coefficients in this expansion can be extracted from the PEMD. On the other hand, these coefficients are determined by $M + 1$ absolute values of the head-on amplitudes $f_{m'}$ with $m' = 0, \ldots, M$ and M values of their relative phases. This suggests a great potential for imaging.

VIII. CONCLUSION

We have extended the adiabatic theory [21] to the specific configuration defined by Eqs. (8)–(10) in which strong-field ionization occurs from a vortex orbital by an elliptically polarized pulse with small ellipticity and the major axis of the polarization ellipse directed along the vortex axis of the initial state. Generation, propagation, and rescattering of vortex electrons in this configuration are described. To this end we have introduced vortex Volkov states in an arbitrary time-dependent homogeneous electric field, Eq. (37), and vortex scattering

states with zero transverse momentum and nonzero impact parameter, Eq. (50), generalizing similar states with zero impact parameter, Eq. (49), introduced in Ref. [28]. Adiabatic asymptotics of the rescattering parts of the wave function, Eq. (59), and the ionization amplitude, Eq. (64), for the present configuration are obtained and the factorization formula, Eq. (72), giving the PEMD in the vicinity of a backward rescattering caustic is derived. The factorization formula generalizes similar formulas derived in Refs. [22,28] to rescattering of vortex electrons with a nonzero impact parameter. It enables one to extract the absolute value of the generalized vortex scattering amplitude defined by Eq. (50) from the observable PEMD, thus extending the approach to target structure imaging initiated in Ref. [3] to yet another target property. The generalized scattering amplitude appearing in the factorization formula (72) is expressed in terms of the head-on vortex scattering amplitudes, Eq. (52). We have shown that in the case of elliptic polarization and the initial π orbital a rich set of information consisting of the absolute values of two head-on amplitudes with $m = 0$ and 1 and their phase difference as functions of the scattering angle θ can be extracted from the PEMD, while in configurations considered previously [22,28] only the absolute value of one scattering amplitude is accessible. We thus conclude that the theory developed in this paper opens a new window for target structure imaging and is expected to find applications in strong-field physics.

ACKNOWLEDGMENTS

APPENDIX: HEAD-ON VORTEX SCATTERING AMPLITUDE FOR SPHERICALLY SYMMETRIC POTENTIALS

For spherically symmetric potentials the head-on vortex scattering amplitude $f_m(k, \theta)$ defined by Eqs. (48) and (49) can be expressed in terms of the usual scattering amplitude $f(k, \theta) \equiv f_0(k, \theta)$ known from scattering theory [57,58]. Here we discuss the relation.

Consider a spherically symmetric potential $V(r)$ which may have a Coulomb tail, $V(r)|_{r \to \infty} = -Z/r$. The usual scattering states for an arbitrary direction of the momentum $\mathbf{k}$ of the incident plane wave are the solutions of the stationary Schrödinger equation

$$\left[-\frac{1}{2}\Delta + V(r) - \frac{1}{2}k^2 \right]\phi(\mathbf{r}; \mathbf{k}) = 0 \qquad (A1)$$

satisfying the boundary condition

$$\phi(\mathbf{r}; \mathbf{k})\big|_{r \to \infty} = e^{i\mathbf{k}\mathbf{r} - i\gamma \ln(kr - \mathbf{k}\mathbf{r})} + f(k, \theta')\frac{e^{ikr + i\gamma \ln 2kr}}{r}, \quad (A2)$$

where $\gamma = Z/k$ and θ' is the angle between vectors $\mathbf{r}$ and $\mathbf{k}$. Similarly to the first line in Eq. (51), we have $r_\perp^{|m|}e^{im\varphi} = (x + i\sigma y)^{|m|}$, where $\sigma = \mathrm{sgn}(m)$. Thus

$$(kr_\perp)^{|m|}e^{im\varphi}e^{ikz} = (-ik)^{|m|}\left(\frac{\partial}{\partial k_x} + i\sigma \frac{\partial}{\partial k_y} \right)^{|m|} e^{i\mathbf{k}\mathbf{r}}\Bigg|_{\mathbf{k}=k\mathbf{e}_z}. \qquad (A3)$$

Using this and comparing Eqs. (49) and (A2), we find

$$f_m(k, \theta)e^{im\varphi} = (-ik)^{|m|}\left(\frac{\partial}{\partial k_x} + i\sigma \frac{\partial}{\partial k_y} \right)^{|m|} f(k, \theta')\Bigg|_{\theta'=\theta}. \qquad (A4)$$

We recall that θ is the angle between $\mathbf{r}$ and the z axis. In calculating the derivatives in Eq. (A4) k can be treated as a constant. Then $f(k, \theta')$ can be considered as a function of a single variable $\cos \theta' = \mathbf{n}\mathbf{n}_k$, where $\mathbf{n} = \mathbf{r}/r$ and $\mathbf{n}_k = \mathbf{k}/k$. Note that the following operators are equal from the point of view of their action on this function:

$$\frac{\partial}{\partial k_x} + i\sigma \frac{\partial}{\partial k_y} = \left[\frac{\partial(\mathbf{n}\mathbf{n}_k)}{\partial k_x} + i\sigma \frac{\partial(\mathbf{n}\mathbf{n}_k)}{\partial k_y} \right] \frac{\partial}{\partial(\mathbf{n}\mathbf{n}_k)}$$
$$= \frac{1}{k} \sin\theta e^{i\sigma\varphi} \frac{\partial}{\partial \cos \theta'}. \qquad (A5)$$

We thus obtain

$$f_m(k, \theta) = (-i \sin\theta)^{|m|} \frac{\partial^{|m|}}{(\partial \cos\theta)^{|m|}} f(k, \theta). \qquad (A6)$$

This formula enables one to calculate $f_m(k, \theta)$ by differentiating the usual amplitude $f(k, \theta)$. For a purely Coulomb potential, $V(r) = -Z/r$, the usual amplitude is given by [57,58]

$$f^{(C)}(k, \theta) = \frac{Ze^{2i\gamma \ln \sin(\theta/2) + 2i\eta_0}}{2k^2 \sin^2(\theta/2)}, \qquad (A7)$$

where

$$\eta_l = \arg \Gamma(l + 1 - i\gamma). \qquad (A8)$$

Substituting this into Eq. (A6) leads to Eq. (55), which was obtained in Ref. [28] by explicitly solving Eq. (A1) with the boundary condition (49). For a general potential with a Coulomb tail Eqs. (A1) and (A2) can be solved using the partial-wave expansion [70]. The scattering amplitude in this case can be presented in the form [57,58]

$$f(k, \theta) = f^{(C)}(k, \theta) + \frac{1}{2ik} \sum_{l=0}^{\infty}(2l + 1)$$
$$\times e^{2i\eta_l}(e^{2i\delta_l} - 1)P_l(\cos\theta), \qquad (A9)$$

where δ_l are phases appearing in the asymptotics $\propto r^{-1}\sin(kr + \gamma \ln 2kr - \frac{1}{2}\pi l + \eta_l + \delta_l)$ of radial functions and $P_l(x)$ are the Legendre polynomials [62]. Substituting Eq. (A9) into Eq. (A6) gives

$$f_m(k, \theta) = f_m^{(C)}(k, \theta) + \frac{i^{|m|}}{2ik} \sum_{l=0}^{\infty}(2l + 1)$$
$$\times e^{2i\eta_l}(e^{2i\delta_l} - 1)P_l^{|m|}(\cos\theta), \qquad (A10)$$

where $P_l^m(x)$ are the associated Legendre polynomials [62]. This formula generalizes the partial-wave expansion (A9) of the usual scattering amplitude [70] to the head-on vortex scattering amplitude. It is the working formula suitable for practical calculations of $f_m(k, \theta)$.

[1] P. B. Corkum, Plasma Perspective on Strong Field Multiphoton Ionization, Phys. Rev. Lett. **71**, 1994 (1993).

[2] M. Meckel, D. Comtois, D. Zeidler, A. Staudte, D. Pavičić, H. C. Bandulet, H. Pépin, J. C. Kieffer, R. Dörner, D. M. Villeneuve, and P. B. Corkum, Laser-induced electron tunneling and diffraction, Science **320**, 1478 (2008).

[3] T. Morishita, A.-T. Le, Z. Chen, and C. D. Lin, Accurate Retrieval of Structural Information from Laser-Induced Photoelectron and High-Order Harmonic Spectra by Few-Cycle Laser Pulses, Phys. Rev. Lett. **100**, 013903 (2008).

[4] M. Okunishi, T. Morishita, G. Prümper, K. Shimada, C. D. Lin, S. Watanabe, and K. Ueda, Experimental Retrieval of Target Structure Information from Laser-Induced Rescattered Photoelectron Momentum Distributions, Phys. Rev. Lett. **100**, 143001 (2008).

[5] D. Ray, B. Ulrich, I. Bocharova, C. Maharjan, P. Ranitovic, B. Gramkow, M. Magrakvelidze, S. De, I. V. Litvinyuk, A. T. Le, T. Morishita, C. D. Lin, G. G. Paulus, and C. L. Cocke, Large-Angle Electron Diffraction Structure in Laser-Induced Rescattering from Rare Gases, Phys. Rev. Lett. **100**, 143002 (2008).

[6] S. Micheau, Z. Chen, A. T. Le, J. Rauschenberger, M. F. Kling, and C. D. Lin, Accurate Retrieval of Target Structures and Laser Parameters of Few-Cycle Pulses from Photoelectron Momentum Spectra, Phys. Rev. Lett. **102**, 073001 (2009).

[7] D. B. Milošević, W. Becker, M. Okunishi, G. Prümper, K. Shimada, and K. Ueda, Strong-field electron spectra of rare-gas atoms in the rescattering regime: enhanced spectral regions and a simulation of the experiment, J. Phys. B **43**, 015401 (2009).

[8] M. Okunishi, H. Niikura, R. R. Lucchese, T. Morishita, and K. Ueda, Extracting Electron-Ion Differential Scattering Cross Sections for Partially Aligned Molecules by Laser-Induced Rescattering Photoelectron Spectroscopy, Phys. Rev. Lett. **106**, 063001 (2011).

[9] C. I. Blaga, J. Xu, A. D. DiChiara, E. Sistrunk, K. Zhang, P. Agostini, T. A. Miller, L. F. DiMauro, and C. D. Lin, Imaging ultrafast molecular dynamics with laser-induced electron diffraction, Nature (London) **483**, 194 (2012).

[10] J. Xu, C. I. Blaga, A. D. DiChiara, E. Sistrunk, K. Zhang, Z. Chen, A.-T. Le, T. Morishita, C. D. Lin, P. Agostini, and L. F. DiMauro, Laser-Induced Electron Diffraction for Probing Rare Gas Atoms, Phys. Rev. Lett. **109**, 233002 (2012).

[11] C. Wang, M. Okunishi, R. R. Lucchese, T. Morishita, O. I. Tolstikhin, L. B. Madsen, K. Shimada, D. Ding, and K. Ueda, Extraction of electron-ion differential scattering cross sections for C_2H_4 by laser-induced rescattering photoelectron spectroscopy, J. Phys. B **45**, 131001 (2012).

[12] M. Okunishi, R. Lucchese, T. Morishita, and K. Ueda, Rescattering photoelectron spectroscopy of small molecules, J. Electron Spectrosc. Relat. Phenom. **195**, 313 (2014).

[13] B. Wolter, M. G. Pullen, M. Baudisch, M. Sclafani, M. Hemmer, A. Senftleben, C. D. Schröter, J. Ullrich, R. Moshammer, and J. Biegert, Strong-Field Physics with Mid-IR Fields, Phys. Rev. X **5**, 021034 (2015).

[14] B. Wolter, M. G. Pullen, A.-T. Le, M. Baudisch, K. Doblhoff-Dier, A. Senftleben, M. Hemmer, C. D. Schröter, J. Ullrich, T. Pfeifer, R. Moshammer, S. Gräfe, O. Vendrell, C. D. Lin, and J. Biegert, Ultrafast electron diffraction imaging of bond breaking in di-ionized acetylene, Science **354**, 308 (2016).

[15] K. Amini, M. Sclafani, T. Steinle, A.-T. Le, A. Sanchez, C. Müller, J. Steinmetzer, L. Yue, J. R. Martínez Saavedra, M. Hemmer, M. Lewenstein, R. Moshammer, T. Pfeifer, M. G. Pullen, J. Ullrich, B. Wolter, R. Moszynski, F. J. García de Abajo, C. D. Lin, S. Gräfe *et al.*, Imaging the Renner-Teller effect using laser-induced electron diffraction, Proc. Natl. Acad. Sci. USA **116**, 8173 (2019).

[16] E. T. Karamatskos, G. Goldsztejn, S. Raabe, P. Stammer, T. Mullins, A. Trabattoni, R. R. Johansen, H. Stapelfeldt, S. Trippel, M. J. J. Vrakking, J. Küpper, and A. Rouzée, Atomic-resolution imaging of carbonyl sulfide by laser-induced electron diffraction, J. Chem. Phys. **150**, 244301 (2019).

[17] M. V. Frolov, N. L. Manakov, and A. F. Starace, Analytic formulas for above-threshold ionization or detachment plateau spectra, Phys. Rev. A **79**, 033406 (2009).

[18] A. Čerkić, E. Hasović, D. B. Milošević, and W. Becker, High-order above-threshold ionization beyond the first-order born approximation, Phys. Rev. A **79**, 033413 (2009).

[19] O. I. Tolstikhin, T. Morishita, and S. Watanabe, Adiabatic theory of ionization of atoms by intense laser pulses: One-dimensional zero-range-potential model, Phys. Rev. A **81**, 033415 (2010).

[20] M. V. Frolov, D. V. Knyazeva, N. L. Manakov, A. M. Popov, O. V. Tikhonova, E. A. Volkova, M.-H. Xu, L.-Y. Peng, L.-W. Pi, and A. F. Starace, Validity of Factorization of the High-Energy Photoelectron Yield in Above-Threshold Ionization of an Atom by a Short Laser Pulse, Phys. Rev. Lett. **108**, 213002 (2012).

[21] O. I. Tolstikhin and T. Morishita, Adiabatic theory of ionization by intense laser pulses: Finite-range potentials, Phys. Rev. A **86**, 043417 (2012).

[22] T. Morishita and O. I. Tolstikhin, Adiabatic theory of strong-field photoelectron momentum distributions near a backward rescattering caustic, Phys. Rev. A **96**, 053416 (2017).

[23] H. Geiseler, N. Ishii, K. Kaneshima, F. Geier, T. Kanai, O. I. Tolstikhin, T. Morishita, and J. Itatani, Carrier-envelope phase mapping in laser-induced electron diffraction, Phys. Rev. A **94**, 033417 (2016).

[24] Y. Ito, M. Okunishi, T. Morishita, O. I. Tolstikhin, and K. Ueda, Rescattering photoelectron spectroscopy of heterodiatomic molecules with an analytical returning photoelectron wave packet, Phys. Rev. A **97**, 053411 (2018).

[25] M. Okunishi, Y. Ito, V. Sharma, S. Aktar, K. Ueda, R. R. Lucchese, A. I. Dnestryan, O. I. Tolstikhin, S. Inoue, H. Matsui, and T. Morishita, Rescattering photoelectron spectroscopy of the CO_2 molecule: Progress towards experimental discrimination between theoretical target-structure models, Phys. Rev. A **100**, 053404 (2019).

[26] T. Mizuno, N. Ishii, T. Kanai, P. Rosenberger, D. Zietlow, M. F. Kling, O. I. Tolstikhin, T. Morishita, and J. Itatani, Observation of the quantum shift of a backward rescattering caustic by carrier-envelope phase mapping, Phys. Rev. A **103**, 043121 (2021).

[27] T. Mizuno, T. Yang, T. Kurihara, N. Ishii, T. Kanai, O. I. Tolstikhin, T. Morishita, and J. Itatani, Comparative study of photoelectron momentum distributions from Kr and CO_2 near a backward rescattering caustic by carrier-envelope-phase mapping, Phys. Rev. A **107**, 033101 (2023).

[28] O. I. Tolstikhin and T. Morishita, Strong-field ionization, rescattering, and target structure imaging with vortex electrons, Phys. Rev. A **99**, 063415 (2019).

[29] J. Harris, V. Grillo, E. Mafakheri, G. C. Gazzadi, S. Frabboni, R. W. Boyd, and E. Karimi, Structured quantum waves, Nature Phys. **11**, 629 (2015).

[30] K. Bliokh, I. Ivanov, G. Guzzinati, L. Clark, R. Van Boxem, A. Béché, R. Juchtmans, M. Alonso, P. Schattschneider, F. Nori, and J. Verbeeck, Theory and applications of free-electron vortex states, Phys. Rep. **690**, 1 (2017).

[31] S. M. Lloyd, M. Babiker, G. Thirunavukkarasu, and J. Yuan, Electron vortices: Beams with orbital angular momentum, Rev. Mod. Phys. **89**, 035004 (2017).

[32] R. Van Boxem, B. Partoens, and J. Verbeeck, Rutherford scattering of electron vortices, Phys. Rev. A **89**, 032715 (2014).

[33] R. Van Boxem, B. Partoens, and J. Verbeeck, Inelastic electron-vortex-beam scattering, Phys. Rev. A **91**, 032703 (2015).

[34] V. Serbo, I. P. Ivanov, S. Fritzsche, D. Seipt, and A. Surzhykov, Scattering of twisted relativistic electrons by atoms, Phys. Rev. A **92**, 012705 (2015).

[35] I. P. Ivanov, D. Seipt, A. Surzhykov, and S. Fritzsche, Elastic scattering of vortex electrons provides direct access to the Coulomb phase, Phys. Rev. D **94**, 076001 (2016).

[36] V. P. Kosheleva, V. A. Zaytsev, A. Surzhykov, V. M. Shabaev, and T. Stöhlker, Elastic scattering of twisted electrons by an atomic target: Going beyond the Born approximation, Phys. Rev. A **98**, 022706 (2018).

[37] A. V. Maiorova, S. Fritzsche, R. A. Müller, and A. Surzhykov, Elastic scattering of twisted electrons by diatomic molecules, Phys. Rev. A **98**, 042701 (2018).

[38] I. P. Ivanov, Promises and challenges of high-energy vortex states collisions, Prog. Part. Nucl. Phys. **127**, 103987 (2022).

[39] D. V. Karlovets, Electron with orbital angular momentum in a strong laser wave, Phys. Rev. A **86**, 062102 (2012).

[40] A. G. Hayrapetyan, O. Matula, A. Aiello, A. Surzhykov, and S. Fritzsche, Interaction of Relativistic Electron-Vortex Beams with Few-Cycle Laser Pulses, Phys. Rev. Lett. **112**, 134801 (2014).

[41] J. M. Ngoko Djiokap, S. X. Hu, L. B. Madsen, N. L. Manakov, A. V. Meremianin, and A. F. Starace, Electron Vortices in Photoionization by Circularly Polarized Attosecond Pulses, Phys. Rev. Lett. **115**, 113004 (2015).

[42] N. V. Larionov, D. N. Makarov, A. A. Smirnovsky, and S. Y. Ovchinnikov, Formation of quantum vortices at the ionization of an atom by an ultrashort laser pulse: Two- and three-dimensional cases, JETP **129**, 949 (2019).

[43] J.-H. Chen, X.-R. Xiao, S.-F. Zhao, and L.-Y. Peng, Dependence of direct and rescattered photoelectron spectra of fluorine anions on orbital symmetry in a short laser pulse, Phys. Rev. A **101**, 033409 (2020).

[44] F. Cajiao Vélez, J. Z. Kamiński, and K. Krajewska, Generation of propagating electron vortex states in photodetachment of H⁻, Phys. Rev. A **101**, 053430 (2020).

[45] F. Cajiao Vélez, L. Geng, J. Z. Kamiński, L.-Y. Peng, and K. Krajewska, Vortex streets and honeycomb structures in photodetachment driven by linearly polarized few-cycle laser pulses, Phys. Rev. A **102**, 043102 (2020).

[46] L. Geng, F. Cajiao Vélez, J. Z. Kamiński, L.-Y. Peng, and K. Krajewska, Vortex structures in photodetachment by few-cycle circularly polarized pulses, Phys. Rev. A **102**, 043117 (2020).

[47] L. Geng, F. Cajiao Vélez, J. Z. Kamiński, L.-Y. Peng, and K. Krajewska, Structured photoelectron distributions in photodetachment induced by trains of laser pulses: Vortices versus spirals, Phys. Rev. A **104**, 033111 (2021).

[48] A. S. Maxwell, G. S. J. Armstrong, M. F. Ciappina, E. Pisanty, Y. Kang, A. C. Brown, M. Lewenstein, and C. F. de Morisson Faria, Manipulating twisted electrons in strong-field ionization, Faraday Discuss. **228**, 394 (2021).

[49] Y. Kang, E. Pisanty, M. Ciappina, M. Lewenstein, C. Figueira de Morisson Faria, and A. S. Maxwell, Conservation laws for electron vortices in strong-field ionisation, Eur. Phys. J. D **75**, 199 (2021).

[50] A. S. Maxwell, L. B. Madsen, and M. Lewenstein, Entanglement of orbital angular momentum in non-sequential double ionization, Nature Commun. **13**, 4706 (2022).

[51] X. B. Planas, A. Ordóñez, M. Lewenstein, and A. S. Maxwell, Ultrafast Imaging of Molecular Chirality with Photoelectron Vortices, Phys. Rev. Lett. **129**, 233201 (2022).

[52] S. G. Walt, N. Bhargava Ram, M. Atala, N. I. Shvetsov-Shilovski, A. von Conta, D. Baykusheva, M. Lein, and H. J. Wörner, Dynamics of valence-shell electrons and nuclei probed by strong-field holography and rescattering, Nature Commun. **8**, 15651 (2017).

[53] F. Schell, T. Bredtmann, C. P. Schulz, S. Patchkovskii, M. J. J. Vrakking, and J. Mikosch, Molecular orbital imprint in laser-driven electron recollision, Sci. Adv. **4**, eaap8148 (2018).

[54] D. Pengel, S. Kerbstadt, D. Johannmeyer, L. Englert, T. Bayer, and M. Wollenhaupt, Electron Vortices in Femtosecond Multiphoton Ionization, Phys. Rev. Lett. **118**, 053003 (2017).

[55] D. Pengel, S. Kerbstadt, L. Englert, T. Bayer, and M. Wollenhaupt, Control of three-dimensional electron vortices from femtosecond multiphoton ionization, Phys. Rev. A **96**, 043426 (2017).

[56] M. Han, J.-B. Ji, T. Balčiūnas, K. Ueda, and H. J. Wörner, Attosecond circular-dichroism chronoscopy of electron vortices, Nature Phys. **19**, 230 (2023).

[57] L. D. Landau and E. M. Lifshitz, *Quantum Mechanics, Non-Relativistic Theory* (Pergamon, Oxford, 1977)

[58] R. G. Newton, *Scattering Theory of Waves and Particles* (Springer-Verlag, New York, 1982).

[59] F. Krausz and M. Ivanov, Attosecond physics, Rev. Mod. Phys. **81**, 163 (2009).

[60] P. A. Batishchev, O. I. Tolstikhin, and T. Morishita, Atomic Siegert states in an electric field: Transverse momentum distribution of the ionized electrons, Phys. Rev. A **82**, 023416 (2010).

[61] O. I. Tolstikhin, T. Morishita, and L. B. Madsen, Theory of tunneling ionization of molecules: Weak-field asymptotics including dipole effects, Phys. Rev. A **84**, 053423 (2011).

[62] M. Abramowitz and I. A. Stegun, *Handbook of Mathematical Functions with Formulas, Graphs, and Mathematical Tables* (Dover, New York, 1964).

[63] D. A. Varshalovich, A. N. Moskalev, and V. K. Khersonskii, *Quantum Theory of Angular Momentum* (World Scientific, Singapore, 1988).

[64] L. V. Keldysh, Ionization in the field of a strong electromagnetic wave, Zh. Eksp. Teor. Fiz. **47**, 1945 (1964) [Sov. Phys. JETP **20**, 1307 (1965)].

[65] D. M. Wolkow, Über eine klasse von lösungen der Diracschen gleichung, Z. Phys. **94**, 250 (1935).

[66] R. P. Feynman and A. R. Hibbs, *Quantum Mechanics and Path Integrals* (McGraw-Hill Companies, New York, 1965).

[67] G. N. Watson, *A Treatise on the Theory of Bessel Functions* (Cambridge University Press, New York, 1944).

[68] G. G. Paulus, W. Becker, W. Nicklich, and H. Walther, Rescattering effects in above-threshold ionization: a classical model, J. Phys. B **27**, L703 (1994).

[69] V. H. Trinh, O. I. Tolstikhin, L. B. Madsen, and T. Morishita, First-order correction terms in the weak-field asymptotic theory of tunneling ionization, Phys. Rev. A **87**, 043426 (2013).

[70] H. Faxén and J. P. Holtsmark, Beitrag zur theorie des durchganges langsamer elektronen durch gase, Z. Phys. **45**, 307 (1927).